

Fermilab Proposal No. 637

Spokesmen:

V. V. Ammosov

IHEP, Serpukhov, USSR

V. S. Kaftanov

ITEP, Moscow, USSR

PROPOSAL TO STUDY NEUTRINO AND ANTINEUTRINO INTERACTIONS
IN DEUTERIUM WITH 15-FT BUBBLE CHAMBER
AT TEVATRON ENERGIES

V. V. Ammosov, A. G. Denisov, V. A. Gapienko, G. S. Gapienko,
V. I. Klukhin, V. I. Koreshev, P. V. Pitukhin, V. L. Rikov,
V. I. Sirotenko, E. A. Slobodyuk, V. G. Zaetz
Institute of High Energy Physics, Serpukhov, USSR

and

V. I. Efremenko, P. A. Gorichev, V. S. Kaftanov,
S. P. Krutchinin, M. A. Kubantsev, I. V. Makhlueva,
A. V., Fedotov, V. I. Shekelyan, V. G. Shevchenko
Institute of Theoretical and Experimental Physics
Moscow, USSR

April 1980

ABSTRACT

We propose a program for a systematic study of neutrino and antineutrino interactions using the Fermilab 15-foot bubble chamber (BC) at the Tevatron energies. This proposal is based on the use of deuterium filling in the 15-ft bubble chamber which will suppress the fermi-motion and intranuclear cascade effects. Thus we will be able to investigate weak interactions on proton and neutron targets separately.

In conjunction with the 15-ft bubble chamber the following devices are expected to be used: a new internal shower picket fence enabling timing of the interactions, identification of photons and electrons and measurement of their energies; a two-plane EMI (External Muon Identifier); a muon spectrometer to measure the energies of hard muons. In this proposal we also discuss possibilities to improve the focusing and monitoring of the neutrino beam.

To perform this experiment 1.2×10^{19} protons at the beam energy $E_p = 1000$ GeV are required. The proposed statistics consists of about 100K interactions in each of the ν and $\bar{\nu}$ exposures.

The main purpose of this experiment is a systematic study of properties of the hadronic final states and especially the mechanism of gluon jet production.

The physics program also includes a study of the energy dependence of the total cross sections; investigation of general features of the deep inelastic νN and $\bar{\nu} N$ scattering; nucleon structure functions and scaling violations; search for new

particles and phenomena including multilepton events; exclusive channels including those with a π^0 's; detailed study of the structure of the weak neutral current.

I. INTRODUCTION

The study of neutrino (antineutrino) interactions has a major role in the research programs of the high energy accelerators. Some of the experiments have been completed,¹ the others are in progress.² Operation of the 1 TeV proton accelerator at FNAL extends experimental possibilities for investigation of the weak interactions with neutrino beams to the incident neutrino energies of $E_\nu > 200$ GeV.

The use of a large bubble chamber (BC) as a detector brings a significant extension to the range of problems which can be solved in neutrino experiments. A detailed picture of an interaction provided by the bubble chamber is essential for the careful studies of the hadronic final states which is not provided by the electronic detectors. However, up to now statistics obtained in a typical neutrino experiment with a bubble chamber is less than 10K events.

Here we propose to continue the systematic investigation of neutrino/antineutrino-nucleon interactions and concentrate mainly on studies of the hadronic final states with statistics of about 100K events using wide band ν_μ and $\bar{\nu}_\mu$ beams.

The Fermilab 15-ft bubble chamber, as the basic detector, will be filled with deuterium. To provide interaction time coincidences, to identify electrons and to measure gamma energies we propose to construct a new Internal Shower Picket Fence (ISPF)³ with about 2π and $\pm 45^\circ$ acceptance for horizontal and vertical directions, respectively. We expect that the new ISPF will be able to measure photon energies with a reliable accuracy

and efficiency. The new ISPF should be installed instead of the present IPF.⁴

To select charged current interactions the present 2-plane External Muon Identifier (EMI)^{5,6} will be used. To measure the energy of the fast muons ($p_\mu > 150$ GeV/c) we propose to use an External Muon Spectrometer.⁷

The use of the deuterium filling will allow us to separate interactions off protons and neutrons.

It is important to concentrate the data handling to a single experimental collaboration which has possibilities for a comparable analysis of the $\nu_\mu N$ and $\bar{\nu}_\mu N$ data.

The proposed experiment will allow:

1. to study general properties of the hadronic final states including properties of the quark and gluon jets;
2. to investigate multilepton final states with soft electrons;
3. to obtain new data for energy dependence of the νp , νn , $\bar{\nu} p$ and $\bar{\nu} n$ charged current cross sections in a wide energy interval (10 - 500 GeV);
4. to study general properties of the deep inelastic ν and $\bar{\nu}$ scattering on proton and neutron target separately;
5. to investigate the structure functions $[F_1^k(x, Q^2)]$, $i=1,3$, $k = \nu p, \nu n, \bar{\nu} p, \bar{\nu} n$ and the scaling violations;
6. to provide an excellent possibility to study the exclusive neutrino processes with π^0 mesons in the final state;
7. to search for new short-lived particles;

8. to study hadronic final states in the νN and $\bar{\nu} N$ neutral current interactions.

We are interested in collaborating with other groups to perform this experiment. The collaboration would enable to us to complete the data handling stage in a reasonable short period of time.

This proposal may be overlapping with other proposals for bubble chamber neutrino experiments. New experimental results which will be obtained in e^+e^- , νN and μN experiments in the near future may introduce some changes to this proposal.

II. EXPERIMENTAL LAYOUT

2.1 Bubble Chamber

As a basic detector we propose to use the Fermilab 15-ft bubble chamber filled with deuterium for the study of neutrino interactions at Tevatron energies. Such filling allow us to suppress fermi motion and intranuclear cascade effects of complex targets and to study neutrino interactions off proton and neutron targets separately.

The fiducial volume of 17m^3 can be chosen to analyze neutrino events (radius $R = 165$ cm and potential length $L_{\text{pot}} > 65$ cm).

The relative error in momentum for bubble chamber track measurements is given as follows:

$$\Delta p/p = 3.6 \text{ } \mu\epsilon / (HL^2),$$

where p -particle momentum (GeV/c), H magnetic field (KG), L -track length (m), ϵ space track setting error in space (mkm). For the track length of 2 m and $\epsilon = 300$ mkm the bubble chamber allows to measure the charged track momentum with better than 10% accuracy up to the momentum of $p = 150$ GeV/c. The bubble chamber can thus provide good measurements of the track momentum for the whole interval of charged hadron momenta.

2.2 External Muon Identifier (EMI)

The present two-plane EMI⁵ will be used for muon identification. The overall geometrical EMI efficiency is expected to be 96% at Tevatron energies. The combined electronic EMI efficiency (with the new ISPF) is expected to be about 92%.

2.3 External Muon Spectrometer

We have shown above (see Sect. 2.1) that the bubble chamber can provide the accuracy of about 10% for the measurements of muon momenta less than 150 GeV/c. To measure momenta of fast muons we intend to use an external muon spectrometer.⁷ Such a spectrometer can be constructed from an array of toroidal iron magnets and drift chambers. The muon momentum will be measured by observing magnetic deflection of the muon track traversing the toroid spectrometer. The average magnetic field of 15 kG can be achieved for coil current about 700 A. For toroid thickness ~ 20 cm and a drift chamber resolution ~ 200 mkm the spectrometer momentum resolution is

$$\frac{\Delta p_{\mu}}{p_{\mu}} = \left[\left(\frac{0.3}{\sqrt{n}} \right)^2 + \left(\frac{0.03 p_{\mu}}{n^2} \right)^2 \right]^{1/2},$$

where n is the number of modules. Thus for n equals 20 the momentum resolution will be about 10% for the muon momentum up to 500 GeV/c.

2.4 Internal Shower Picket Fence (ISPF)

The present IPF⁴ for the Fermilab 15-ft bubble chamber is used to determine the time of a neutrino event inside the bubble chamber and has relatively low electronic efficiency of about 70-80%. We propose to build a new ISPF which also would be placed in the vacuum tank between the bubble chamber body and the superconducting magnet.

The new feature of this detector is the possibility to measure the electron/gamma energies and to separate electrons

from hadrons. For these purposes the measurement of the number of particles in the maximum of an electromagnetic shower can be used.

To decrease the influence of a strong $E \times B$ effect the new ISPF would consist of a large number of high pressure argon or xenon ionization chambers. The ionization chambers will be made from 10 mm diameter stainless steel tubes. The detector will have 2π azimuthal acceptance and $\pm 45^\circ$ vertical acceptance for 3 m tube length. An additional Pb or W convertor just in front of the tubes would be installed to achieve the total of about 5-6 radiation lengths together with the 1" stainless steel bubble chamber vessel. Minimum mechanical reconstruction will be needed to assemble the new detector.

We expect the following parameters of the new ISPF:

- the energy resolution for electron/gamma showers $\Delta E/E$ (FWHM) = $0.75/\sqrt{E}$;
- the electron-hadron separation efficiency less than 5%;
- the electronics efficiency about 99%;
- the time resolution about 0.5-1.0 μ sec.

Besides this new ISPF will be able to associate secondary neutral objects (N-stars, V^0 's) with primary neutrino interactions. The 2π azimuthal acceptance will provide high selection between neutrino neutral current events and neutral hadron interactions induced by neutrinos in the magnet coils and other upstream materials.

The results of the prototype test of the proposed ISPF will be presented separately.

The general layout of the Fermilab 15-ft bubble chamber with the external devices is shown in Fig. 1. The expected energy and angular resolutions are discussed in Appendix II.

2.5 Neutrino Fluxes and Expected Event Yields

We propose an exposure of the 15-ft bubble chamber to wide-band neutrino and antineutrino beams. Here we consider the use of the "beam guide" focusing system with a central conductor (wire)³⁸ in the present decay pipe as one possibility for the focusing system. The details of the description of this system and the corresponding calculated neutrino and antineutrino fluxes are given in Appendix I.

The ν and $\bar{\nu}$ fluxes obtained using one horn system and proposed wire focusing system are identical, within errors, according to our calculations (Figs. 2 and 3). However, the wire focusing system enables deflection of the π and K mesons of a n opposite charges in the whole length of the decay pipe. This is important for the composition of the antineutrino beams. To suppress the neutrino contamination in the plug is not needed and consequently the antineutrino flux can be enhanced in the high energy part of the spectrum ($E_{\bar{\nu}} > 100$ GeV by a factor of 2 (see Fig. 3).

Purity of the neutrino fluxes is essential for the study of neutral current neutrino interactions. The proposed system will provide the maximum neutrino fluxes at the minimal contamination from wrong type neutrinos.

Note, that the wire focusing system does not impose as strong restrictions on the focusing element itself as the horn system does, during the Tevatron fast spill time of 2 msec.

The expected charged-current event yields in the 17m^3 fiducial volume of the 15-ft bubble chamber at intensity of 10^{13} ppp are given in Table I. We propose to carry out this experiment with event statistics of about 100K events both in neutrino and antineutrino exposures, i.e. exposures of 2×10^{18} protons for the neutrino beam and 10^{19} protons for the anti-neutrino beam are required.

Using the expected parameters of the Tevatron ($I = 2 \times 10^{13}$ ppp, cycle time 60 sec) we estimate that 500 days are needed to take the total event sample. The required statistics can be taken during 3 years with 2 runs per year lasting about 2.5-3 months each.

To suppress by a factor of 5 the event yield in the soft part of a neutrino flux ($E_\nu < 100$ GeV) a collimator with $\theta < 3$ mrad after the target can be used. The high energy part of the neutrino spectrum will not change significantly (10-20%).

2.6 Neutrino Beam Monitoring

To determine the total neutrino cross-sections and to study the absolute values of structure functions it is desirable to know the ν_μ and $\bar{\nu}_\mu$ fluxes with an accuracy of about 5-10%.

To fulfill this program the measurement of π and K yields from the real neutrino target would be done. The neutrino flux reconstruction can be made using muon flux measurements.

The measurements of muon momenta and angular distributions can be carried out with an array of standard magnets and drift chambers with a total magnetic length of 15 Tm. This system can be used for proton intensity up to 10^{10} protons/sec.

An ionization chamber system installed in 3-4 arrays of the iron shield can be used to integrate the muon intensity and to check the operation of the neutrino channel during an exposure.

III. PHYSICS

3.1 Analysis of Properties of the Hadronic Final States

The systematic investigation of hadronic final states in the wide intervals of hadronic center-of-mass energies W and lepton 4-momenta transferred, Q^2 , is one of the basic goals of this experiment. At the Tevatron energies these intervals are

$$1 < W^2 < 900 \text{ GeV}^2 \text{ and } 0 < Q^2 < 500 \text{ (GeV/c)}^2.$$

The 15-ft bubble chamber will provide reasonable momentum resolution $\Delta p_h/p_h \sim 5\text{-}6\%$ and angular resolution $\Delta\theta \sim 3$ mrad for the charged hadron measurements. The new ISPF will give high (99%) electron/gamma detection efficiency and energy resolution about $75/(E)^{1/2}\%$ (FWHM). Monte-Carlo calculations show (see Appendix II) that the combined BC + ISPF detector will enable the measurement of the total hadronic energy flow with the energy and angular resolutions $\sigma_{E_h}/E_h \sim 10\%$ and $\delta \sim 8$ mrad at high E_h .

3.1a Search for the gluon jets

The gluons begin to play an essential role in the deep inelastic scattering with the increased neutrino energies. Hard gluon bremsstrahlung from the outgoing quark leads to the jet broadening and eventually to the two-jet structure in the current fragmentation region.¹⁵

About 2.5% of all charged current interactions (or 2500 events) will have a high invariant mass of the final hadronic system $20 < W < 30$ GeV and about 7.5% of the events will have $W > 15$ GeV. Thus, a detailed comparison of the gluon jets produced

in neutrino reactions and in e^+e^- annihilation at PEP and PETRA energies is possible.

Theoretical predictions for the jet cross sections as functions of the variables T (thrust) and S (sphericity) have been calculated in the first-order QCD perturbation theory.¹⁶ These variables are defined as

$$T = 2 \max \frac{\tilde{\Sigma} p_{L,i}}{\Sigma |p_i|} \quad (3.1)$$

$$S = \left(\frac{4}{\pi}\right)^2 \min \left(\frac{\Sigma |p_T^i|}{\Sigma |p_i|} \right)^2, \quad (3.2)$$

where Σ_i is a sum over all particles;
 $\tilde{\Sigma}_i$ is a sum over the particles in the hemisphere;

p_L, p_T are longitudinal and transverse momenta with respect to the jet axis determined by (3.5) and (3.6).

For $W > 20$ GeV, the first-order perturbative QCD contribution to the cross section $1/\sigma$ ($d\sigma/dT$) can be separated from the non-perturbative background for $T < 0.73$.¹⁶ A similar separation can be done for the averages $\langle 1 - T \rangle$ and $\langle S \rangle$ as functions of W .

Hard gluon bremsstrahlung also contributes to the angular correlations of hadrons relative to the lepton plane. In particular, azimuthal asymmetry is expected for the averages $\langle \cos \phi \rangle$ and $\langle \cos 2\phi \rangle$,¹⁷ where ϕ is the azimuthal angle of a hadron in the plane transverse to the Q vector.

Effects of the hard gluon bremsstrahlung are expected to be seen also in the angular energy flow.¹⁸

The study of CC events with final-state hadrons having large transverse momenta is also important for the verification of the QCD predictions. QCD predicts a rise of $\langle p_T^2 \rangle$ of hadrons as a function of W^2 and Q^2 .¹⁹ In the selected region $W > 20$ GeV and $T < 0.73$ the first-order QCD contribution is dominant.

The smallness of the nucleon fermi motion in deuterium target and a reasonable energy resolution will enable us to investigate the primordial fermi motion of the initial quarks. To study the primordial transverse momentum we intend to use p_T correlations of the current and target fragments. There is no such possibility in the e^+e^- experiments.

3.1b Study of fragmentation processes and fragmentation function properties

The fragmentation functions are fundamental for the description of the quark fragmentation into observed final-state hadrons.

Neutrino-induced reactions give an ideal possibility for their study due to the possibility to select the initial quark flavor. In the region where the valence quarks dominate ($X_B > 0.1$) the neutrino (antineutrino) interacts almost exclusively with the d(u) quark.

With the standard notation the fragmentation function D_q^h describes the probability that a quark q disintegrates into a hadron h . Isospin and charge-conjugation symmetries reduce the number of independent fragmentation functions to twelve: six for pions and six for kaons.

At present there are only poor experimental data²⁰ for $D_u^{\pi^+}$
 $= D_d^{\pi^-}$, $D_d^{\pi^+} = D_u^{\pi^-}$, $D_u^K_S$, $D_d^K_S$, and D_S^K fragmentation functions.

The proposed experiment will enable us to measure three remaining fragmentation functions for neutral pions ($D_u^{\pi^0}$, $D_d^{\pi^0}$, $D_S^{\pi^0}$) and to improve present results. The combined ν and $\bar{\nu}$ analysis will be needed to measure $D_S^{\pi^0}$.

There will also be a possibility to investigate the factorization and scaling properties of the fragmentation functions in this experiment.

The QCD predicts factorization of the single-particle inclusive distributions as follows:²¹

$$\frac{d^2\sigma}{dxdz} = \sum_i q_i(x, Q^2) D_i^h(z, Q^2),$$

where q_i are quark (antiquark) distributions and D_i^h is a fragmentation function. The region where factorization holds is provided by

$$\alpha_S/\pi \ll 1; \ln Q^2/\Lambda^2 \gg \ln x, \ln(1-x), \ln z, \ln(1-z).$$

In this region QCD predicts a logarithmic Q^2 evolution for the z moments of the fragmentation functions.²²

The proposed experiment will allow us to study both non-singlet moments²³ due to the quark fragmentation mechanism and singlet moments²⁴ due to the gluon fragmentation mechanism.

3.2 Multilepton States

Multilepton final states in neutrino (antineutrino) interactions are directly connected to the new phenomena--the heavy quark or lepton production.

There will be a good opportunity to search and study the multilepton events in detail. The bubble chamber provides a full description of the produced hadrons, especially of the neutral strange particles (K_S^0, Λ). On the other hand, external detectors provide high efficiency for the lepton (electron and muon) detection. The two-plane EMI will allow identification of the multilepton events with an efficiency of $\sim 90\%$ for $p > 4$ GeV/c. The new ISPF will enable identification of electrons hitting the ISPF plane with the efficiency of $\sim 95\%$. Moreover, the bubble chamber will enable the identification of direct electrons with $p_e < 1$ GeV/c by their spiralization in the bubble chamber. Use of the deuterium filling suppresses the main sources of background for direct electrons such as closing Compton electrons and closing asymmetrical gamma rays. The lowest electron momentum cut off will be at $p_e > 300$ MeV/c.

The proposed experiment is thus suited to study the μe and μee processes in a wide kinematical range of the electron energies ($p_e > 300$ MeV/c).

Opposite sign dileptons are qualitatively understood²¹ as the decay produces singly charmed mesons; however, the present statistics (especially for the μ^+e^- in antineutrino interactions) should be increased.

Using ~ 500 μe and ~ 500 $\mu\mu$ opposite sign dilepton events in the $\nu/\bar{\nu}$ beams we would investigate:

1. Form of the fragmentation function $D(z)_q^c$ for charmed mesons. Here the low energy cut off for the second lepton is extremely important;

2. The strange quark structure function $f_S(x, Q^2)$. Expectations from the QCD calculations predict a 30% change of $f_S(x, Q^2)$ from $Q^2 = 2$ to 100 (GeV/c).

The study of like-sign dilepton events is connected both with the associated charm-anticharm ($C\bar{C}$) production and b-quark contribution.

The $u \rightarrow b$ ($c \rightarrow b$) transitions in $\bar{\nu}$ interactions and the $\bar{u} \rightarrow \bar{b}$ ($\bar{c} \rightarrow \bar{b}$) transitions in ν -interactions are the main sources of b-quark production. Theoretical estimates for the b-quark production rate in $\nu/\bar{\nu}$ interactions²⁶ give for

$$r = \frac{(\bar{\nu}N \rightarrow \mu^+ b)}{(\bar{\nu}N \rightarrow \mu^+ x)},$$

$r = 5 \times 10^{-4}$ and $r = 10^{-3}$ at $E_{\bar{\nu}}$ = 100 GeV in neutrino and antineutrino scattering, respectively. An antineutrino experiment is thus better in studying b-quark production.

A final-state b-quark disintegrates into B-hadron and then decays. Lepton signals from the b-quark decay have been investigated by many theorists.²⁷ Leptons from the $b \rightarrow c l \nu$ decays have large p_T with respect to the B-hadron direction of flight. We expect ~ 15 semileptonic B decays in the antineutrino and ~ 10 semileptonic B-decays in neutrino interactions.

Trilepton events have created interest because they are considered to be manifestations of the "new physics." It has been shown, however, that at present energies ($E < 200$ GeV) the observed $\mu^- \mu^- \mu^+ \nu$ events²⁸ and the $\mu^+ \mu^+ \mu^- \bar{\nu}$ events²⁹ are due to ordinary charged current events with an additional muon pair from the radiative and hadronic origins. Trilepton events of the kind

$\mu^- \mu^- e^+$ or $\mu^- \mu^+ e^-$ would be of particular interest since they could not be from muon pair "background."

3.3 Inclusive Charged-Current (Anti-) Neutrino Scattering

The kinematics of inclusive charged-current (anti-) neutrino-nucleon scattering

$$\left(\bar{\nu}\right)_+ N \rightarrow \mu^\pm + X \quad (3.3)$$

can be described with three variables:

E_ν = neutrino energy;

$-q^2 = Q^2 = 4E_\nu E_\mu \sin^2 \theta/2$ = square of the four-momentum transfer to the hadronic system;

$\nu = E_h - M \approx E_h$ = energy transfer to the hadronic system or in terms of the scaling variables $X = Q^2/2M\nu$ and $Y = \nu/E_\nu$.

Assuming the V-A form of the weak charged-current interactions the double differential cross section for the process (3.3) has the following form:

$$\frac{d^2 \sigma^{\nu, \bar{\nu}}}{dx dy} = \frac{G^2 M E_\nu}{\pi} \left[(1 - y) F_2(x, Q^2) + \frac{y^2}{2} 2x F_1(x, Q^2) \pm (y - y^2/2) \times x F_3(x, Q^2) \right], \quad (3.4)$$

where the +/- sign refers to neutrino/antineutrino scattering. The three structure functions $F_i(x, Q^2)$ ($i = 1, 2, 3$) contain the dynamics of the process (3.3).

If the Callan-Gross relation $2xF_1 = F_2$ is valid,⁸ then the differential cross section (3.4) has the form:

$$\frac{d^2 \sigma^{\nu, \bar{\nu}}}{dx dy} = \frac{G^2 ME}{\pi} [1/2(1 + (1 - y)^2) F_2(x, Q^2) \pm 1/2 (1 - (1 - y)^2) \times x F_3(x, Q^2)]. \quad (3.5)$$

The structure functions can be extracted from the measured cross sections of the neutrino and antineutrino-nucleon interactions since

$$F_2(x, Q^2) \sim \frac{d^2 \sigma^{\nu}}{dx dy} + \frac{d^2 \sigma^{\bar{\nu}}}{dx dy} \text{ or } F_2(x, Q^2) \sim \frac{d^2 \sigma^{\nu, \bar{\nu}}}{dx dy} \Big|_{y=0}$$

$$x F_3(x, Q^2) \sim \frac{d^2 \sigma^{\nu}}{dx dy} - \frac{d^2 \sigma^{\bar{\nu}}}{dx dy}.$$

With the deuterium target it is easy to separate the (anti-) neutrino interactions off protons and neutrons and thus determine the structure functions $F_2^{\nu n}$, $F_2^{\nu p}$, $x F_3^{\nu n}$, and $x F_3^{\nu p}$ using the assumption of charge symmetry in the neutrino-nucleon scattering, i.e., $F_i^{\bar{\nu} p} = F_i^{\nu n}$ and $F_i^{\nu p} = F_i^{\bar{\nu} n}$.

The scaling hypothesis predicts that

$$F_i(x, Q^2) \xrightarrow[Q^2, \nu \rightarrow \infty]{\text{at fixed } x} F_i(x).$$

The existing experimental data indicate that the deviation from the scaling at moderate Q^2 is about 10%. This experiment gives a possibility to extend the Q^2 range up to 500 GeV² and to verify the scaling hypothesis in the whole Q^2 region.

The verification of violation of the Callan-Gross relation using a wide Q^2 range is of great interest due to unreliability of the existing experimental data.

Knowledge of (anti-) neutrino fluxes with a precision of 10% permits measurement of the behavior of the total cross sections in the new energy range $E_{\nu, \bar{\nu}} > 200$ GeV.

The comparison of νp and $\bar{\nu} p$ data at $X \approx 1$ gives a possibility to verify model predictions for the quark ratio u/d at $X = 1$. For example, in a QPM⁹ $u = 2d$ and in the QCD¹⁰ $u = 5d$ at $X = 1$.

The comparison of νp and $\bar{\nu} p$ data is important also for a verification of the Adler sum rule

$$\int_0^1 \frac{dx}{x} (F_2^{\bar{\nu}p} - F_2^{\nu p}) = 2.$$

The investigation of the Q^2 dependence of the structure functions is important for understanding of the nature of the scaling deviations. The significant Q^2 -dependence of the structure functions observed in eN ¹¹ and μN ¹² experiments can be explained neither by threshold effects connected with production of heavy quarks nor by the target mass effects. On the other hand the asymptotically free field theories predict deviation from Bjorken's scaling, one of them - the quantum chromodynamics (QCD), which claims to a role of theory of strong interactions. In this experiment there is a possibility to verify the quantitative predictions of the QCD with a reasonable accuracy.

For comparison with the QCD, moments of the structure functions are usually used since only for them the QCD gives unambiguous predictions. In a simplest cast N^{th} moment of the structure function F_2 or xF_3 ($F_i(x, Q^2)$) has the form

$$M_i(N, Q^2) = \int_0^1 x^{(N-2)} F_i(x, Q^2) dx \quad (3.6)$$

However, at moderate neutrino energy it is impossible to calculate correctly the integral (3.6) since at a given value of Q^2 the X variable does not cover the whole X interval (0.-1.). At high Q^2 the X values are restricted from below due to natural restriction in neutrino energy ($E_\nu < 200$ GeV). At low Q^2 the X -values are restricted from above because of the E_h selection. For example, by this reason the BEBC group was forced to use the data from Gargamelle for the analysis of the Q^2 - dependence for the structure function moments.¹³ This experiment will cover a wider Q^2 - region (see Fig. 4) and will have a considerable advantage in the study of structure function moments.

Thus, for example, the moments of the "valence" quarks (structure function xF_3) do not depend on the distribution of gluons in the nucleon and these moments have the simplest form in the QCD¹⁴

$$M_3(N, Q^2) = \text{const.} \times (\ln Q^2 / \Lambda^2)^{-d^{NS}}$$

where

$$d^{NS} = \frac{4}{33-2m} \left(1 - \frac{2}{N(N+1)} + 4 \sum_{j=2}^N \frac{1}{j} \right)$$

and m is the number of quark flavors.

It is necessary to note once more that the data on the deep-inelastic $\nu N / \bar{\nu} N$ scattering, obtained in this experiment, will be considerably cleaner than in the counter experiments since with

the use of the deuterium target fermi-motion and intra-nuclear cascade effects are strongly suppressed. The usage of a wide-band $\nu/\bar{\nu}$ -flux enables to cover a wide Q^2 region in a single experiment.

3.4 Study of Exclusive Channels

Up to now little experimental information about exclusive channels exists.

These data would give answers to the following questions:

- what are contributions of individual exclusive channels to the energy dependence of the total cross-sections;
- what is the role of diffractive processes in resonance production;
- what is the role of resonances in generation of scaling violations;
- does the Q^2 - dependence of helicity effects, similar to those found in $eN \rightarrow eN^*$ reactions, exist.

The proposed experiment will give possibilities to answer these questions. The deuterium target will allow to select 3C-fit channels. The ISPF will enable to detect π^0 -mesons in the final states. Thus, there will be possibilities to investigate a great number of exclusive channels including a chance to obtain a detailed information about octet $I=1/2$ and decuplet $I=3/2$ baryon production.

3.5 Study of Neutral Strange Particle Production

The bubble chamber is an ideal detector to observe decays of neutral strange particles (K_S^0 , Λ , \bar{K}). We intend to obtain new

data for inclusive strange particle production and exclusive channels with neutral strange particles. Neutral strange particle production in neutral current $\nu/\bar{\nu}$ interactions is of particular interest. There is practically no experimental data on NC events.

3.6 Study of Neutral Current ν and $\bar{\nu}$ Interactions

The new ISPF will provide 2π azimuthal coverage of the bubble chamber. Charged hadrons from the upstream $\nu/\bar{\nu}$ interactions will give signals in the forward hemisphere of the ISPF and any event induced by secondary neutrals in the bubble chamber will be eliminated directly. For CC events the muon will always penetrate the ISPF and Monte-Carlo calculations show that the overall probability of self-vetoing is about 92%. The time coincidence with K_L^0 or neutron interactions will allow to reduce this background by 65% for the total hadron energy cut $E_h > 5$ GeV. Moreover, the characteristics of this background, i.e., absolute magnitude, energy spectrum, etc., can be determined.

The use of the wire focusing system for secondary mesons would reduce the contamination from background neutral current $\bar{\nu}/\nu$ interactions.

The neutral current interaction of neutrinos with nucleons is presented as

$$L = -\frac{G}{2} \bar{\nu} \gamma_\alpha (1+\gamma_5) \nu [\bar{u} \gamma_\alpha \{u_L(1+\gamma_5) + u_R(1-\gamma_5)\} u + \\ + \bar{d} \gamma_\alpha \{d_L(1+\gamma_5) + d_R(1-\gamma_5)\} d + \dots]$$

It is interesting to measure the couplings u_L, d_L, u_R, d_R ... and to discriminate those between theoretical models. These coupling constants summarize the structure of the neutral current interaction and contain vital information about the properties of intermediate bosons.

The proposed experiment will allow us to obtain new information about the following subjects:

a. Isoscalar-isovector interference

The deuterium target will allow to separate NC interactions on protons and neutrons. A direct probe of the isospin structure is the combined data analysis of ν and $\bar{\nu}$ inclusive cross sections which allows to obtain the estimation of $\Delta_L = u_L^2 - d_L^2$ and

$$\Delta_R = u_R^2 - d_R^2$$

$$\frac{\sigma_{p^-} \sigma_n}{\sigma_{p^+} \sigma_n} \nu \rightarrow \nu = \Delta_L + \frac{1}{3} \Delta_R$$

$$\frac{\sigma_{p^-} \sigma_n}{\sigma_{p^+} \sigma_n} \bar{\nu} \rightarrow \bar{\nu} = 1.9 (\Delta_R + \frac{1}{3} \Delta_L)$$

Measurements of the π^+/π^- ratio in NC and CC semi-inclusive reactions can help to give additional restrictions for the $u_L^2, u_R^2, d_L^2,$ and d_R^2 using the relations:

$$\left(\frac{\pi^+}{\pi^-}\right)_{\nu \rightarrow \mu^-} = D_u^{\pi^+} / D_u^{\pi^-}$$

$$\left(\frac{\pi^+}{\pi^-}\right)_{\bar{\nu} \rightarrow \mu^+} = D_u^{\pi^-} / D_u^{\pi^+}$$

$$\left(\frac{\pi^+}{\pi^-}\right)_{\nu \rightarrow \nu} = \frac{(u_L^2 + \frac{1}{3} u_R^2) D_u^{\pi^+} + (d_L^2 + \frac{1}{3} d_R^2) D_u^{\pi^-}}{(u_L^2 + \frac{1}{3} u_R^2) D_u^{\pi^-} + (d_L^2 + \frac{1}{3} d_R^2) D_u^{\pi^+}}$$

$$\left(\frac{\pi^+}{\pi^-}\right)_{\bar{\nu} \rightarrow \bar{\nu}} = [L \rightarrow R]$$

b. Study of selected exclusive channels.

In almost all of the models based on the GIM mechanism,³⁰ the neutral current is predicted to be symmetric under d-s or u-c interchanges. It is important to determine the NC couplings of the s and c quarks.

The NC coupling to strange quarks can be measured using K_S^0 's in the $\nu/\bar{\nu}$ neutral current interactions. Assuming $\sin^2 \theta_w = 1/4$, parton densities in the proportion $\bar{Q}/Q = 0.1$ and $\bar{Q}_s/\bar{Q} = 1/3$ one finds³¹ that the average multiplicities $\langle n^{K^0 + \bar{K}^0} \rangle$ for $z > 0.5$ are

$\nu \rightarrow \nu$	0.069	with	$s\bar{s}$
	.044	without	$s\bar{s}$
$\bar{\nu} \rightarrow \bar{\nu}$.087	with	$s\bar{s}$
	.039	without	$s\bar{s}$

The $C\bar{C}$ contribution may be estimated using CC events with the wrong sign lepton signature at high y . I.e., an elementary process $\nu c \rightarrow \nu c$ followed by the decay $c \rightarrow s l^+ \nu$ ($\bar{c} \rightarrow \bar{s} l^- \bar{\nu}$) can produce events like $\nu N \rightarrow \mu^+ x, e^+ x$; $\bar{\nu} N \rightarrow \mu^- x, e^- x$. The ISPF for electrons and the wire focusing system may help to solve this problem.

c. Diffractive Production of Mesons.

Diffractive production of vector and axial vector mesons is a direct way to determine the quantum number's of the neutral current. In the presence of an $\bar{s}s$ component in the NC one expects the following proportion for their production³¹

$$A_1^0 : \rho^0 : \phi^0 : \phi_a^0 = 1:1.2:0.2:0.1.$$

IV. CONCLUSION

The proposed experiment is aimed at a systematic study of neutrino/antineutrino-deuterium interactions at statistics of ~100K events in ν and $\bar{\nu}$ - beams.

The 15-ft bubble chamber, supplemented by ISPF, EMI, and the muon spectrometer, will combine the basic benefits of a bubble chamber and electronic techniques.

This will allow us to obtain a detailed picture of neutrino interactions and provide high electron and muon identification efficiency as well as measurements of electromagnetic component and hard muon momenta.

To accomplish our physical program we require the total number of protons of 2×10^{18} and 10^{19} in a ν and $\bar{\nu}$ exposures, respectively. With the proton beam intensity $I = 2 \times 10^{13}$ ppp, the neutrino exposure will take about 80 days of the bubble chamber operation and the antineutrino one ~400 days.

It is expedient to take the total neutrino statistics in the first run of the experiment which should continue during three months. As to the antineutrino statistics, we suggest that it should be taken in subsequent exposures.

For scanning and measuring we can use 10 projectors with low (15 \times) and high (60 \times) magnification, one or two automatic CRT's, and one HPD. Our experience in 15-ft bubble chamber film data handling in previous experiments E-180 and E-564 indicates that the scanning rate is about 200 frames/day per device and the measurement rate is about 25 events/day per device.

Our contribution into the construction of the 15-ft bubble chamber hybrid system could be the following:

1. manufacture and test of ISPF ionization chamber pickets;
2. development and production of high pressure gas system;
3. participation in the development and production of channels of electronics based on combined radio-components.

If Fermilab makes a decision to modify the neutrino channel, we are ready to consider a possibility to participate in these efforts.

To have all the work on the 15-ft bubble chamber hybrid system accomplished and the film analyzed in a reasonably short period of time, we are interested in this experiment to be carried out in collaboration with other laboratories.

APPENDIX I

Wide-band neutrino and antineutrino beams at the Tevatron

A wide-band meson focusing for neutrino beams has some peculiarities at high energy. Magnetic horns³² and parabolic lenses,³³ widely used now, become ineffective and, moreover, their utilization causes significant technical difficulties.

The main reason of horn inefficiency is that at high energies the fraction of secondary mesons with small production angles increases extremely and, therefore, a magnetic field does not deflect them. Consequently the background of wrong sign mesons increases considerably. The use of the plug for the background suppression decreases the neutrino flux from right sign mesons especially in unknown high energy part of spectra which should be studied.

The design fast spill time for a new generation of high energy fixed target accelerators will be a few msec. In this case the high current pulse of the horn power supply will cause a significant heating of the horn cover. As was mentioned in Ref. 34, the horn utilization for the Tevatron will require further considerable efforts.

To obtain high intensity neutrino beams at Tevatron energies we propose to use "beam guide" meson focusing system^{36,37} with a thin central conductor along the axis of the decay pipe. The advantages of this focusing system for high energy mesons, which will be called here focusing wire (FW), were discussed in detail in Ref. 38.

The axially symmetrical magnetic field is induced by a current pulse in a thin central conductor (wire) stretched along a full length of the decay pipe. The vacuum tube can be a reverse conductor.

Charged mesons accomplish an oscillatory movement in the radial direction due to the prolonged magnetic field of the focusing wire. The neutrino flux increase is provided by a considerable portion of meson decays which occur in trajectory sections parallel to neutrino channel axis.

To reduce the meson absorption in the wire the transverse dimensions of the proton beam on a neutrino target should be increased. This is also useful for protection of a neutrino target against extensive pulse heating by a high intensity proton beam.

The FW magnetic field has a maximum around the wire and decreases proportionally to $1/r$. The strong magnetic field near the axis reduces the contribution of wrong sign mesons produced at small angles.

As was shown in paper,³⁸ the FW provides a reasonable acceptance for secondary mesons induced by protons with $E_p = 1$ TeV at pulse currents about 1-2 KA. This magnitude is 100 times less than horn current. Due to a low value of the FW current the natural cooling can be provided for a 10-50 msec FW pulse.

Figure 5 shows the integral neutrino flux (1-st curve) and flux densities at fixed E_ν energies (curves 2, 3, 4, 5, 6, 7 and 8 are for $E = 10, 50, 100, 150, 200, 250,$ and 300 GeV, respectively) for the 15-ft bubble chamber as a function of the FW

current assuming the gaussian distribution of the proton beam on a target with $\sigma_p=1$ cm. At the current growth up to 2 kA neutrino fluxes increase and then become a constant.

Figure 6 shows the neutrino flux and flux densities as a function of the proton beam size σ_p (curves 9 and 10 are for $E = 350$ and 400 GeV). It seems that fluxes are independent on σ_p for $\sigma_p > 0.5$ cm.

Figures 7 and 8 show the same background antineutrino fluxes and densities as a function of I_w and σ_p .

It is possible to choose two modes of the focusing:

- to obtain the maximum of the signal/background ratio;
- to obtain the maximum of the basic ν_μ or $\bar{\nu}_\mu$ flux.

The background/signal ratios for a neutrino beam are summarized in Table II as a function of I_w and σ_p .

To calculate the $\nu_\mu/\bar{\nu}_\mu$ fluxes we used a modified NUADA program³⁹ for the focusing wire with the following parameters: $I_w = 2$ KA, $\sigma_p = 1$ cm, $L_w = 400$ m, and $r_w = 1$ mm. For the secondary meson spectra we used the IHEP parametrization⁴⁰ obtained by fitting π and K yields from the thick Al target in the angle range $0 \div 50$ mrad and the momentum range $5 < p < 55$ GeV/c at proton energy 67 GeV/c.⁴¹ Systematic errors for π_\pm and K_\pm mesons are 5% and 10%, respectively.

We choose the invariant cross section in the following form:

$$\frac{E}{p^2} \frac{d^2\sigma}{dpd\Omega} = a_1(1-x)^{a_2} \times \exp(a_3x - a_4\sqrt{x}) \{ (1-a_5)\exp(-a_6p_T^2) + a_5\exp(-a_7p_T^2) \}$$

where E , p and Ω - energy, momentum and solid angle for secondary mesons, $x = 2p^* / \sqrt{S}$, and p_T -meson transverse momentum.

Parameters of this form for an Al target with the length equal to 60 cm and the radius equal to 3 cm are given in Table III and were used for calculation of neutrino fluxes.

The momentum spectra of secondary mesons at 1 TeV proton energy are shown in Fig. 9 for production angle $\theta < 40$ mrad.

A comparison of this and Stefanski-White⁴² parametrizations with the available meson production at 300 GeV/c⁴³ is shown in Fig. 10.

Expected fluxes for neutrino beam are shown in Fig. 2. To make comparison more convenient the correspondent relative fluxes and event yields are given in Table IV. Horn parameters are taken from Ref. 44.

The same fluxes and estimations for antineutrino beam are given in Fig. 3 and Table V.

From Fig. 2 (Fig. 3) one can see that the neutrino (antineutrino) flux is the same for one horn and the FW, but the wrong sign contamination for the FW is 5 times less than for the horn. For the antineutrino beam the use of the plug with horn decreases 2 times the antineutrino flux for the energy greater than 100 GeV.

Some technical and electric parameters of the FW system are given in Table VI for the blacken copper wire. Energy parameters for the FW system are given in Table VII, assuming rectangular current pulses which can be achieved using the method of Ref. 47.

APPENDIX II

Investigation of an experimental accuracy of the bare 15-ft bubble chamber and the bubble chamber equipped with the ISPF has been done by Monte-Carlo simulation of neutrino events. It was assumed that the bubble chamber is filled with deuterium with density 0.14 g/cm^3 , absorption length 300 cm and radiation length 900 cm. The fiducial volume was restricted by 17 m^3 and was chosen so that potential length for secondaries along neutrino direction was greater than 65 cm. The neutrino flux which was used in Monte-Carlo program is shown in Fig. 2.

For the simulation of a lepton vertex in a neutrino event the quark-parton model with Feynman-Field parametrization of quark distributions⁴⁵ was used. For the generation of a hadron system we have used the model of uncorrelated production which was described in detail in Ref.⁴⁶ This model reproduces satisfactorily the main properties of the hadron production in the deep-inelastic neutrino scattering.

The neutrino vertex was determined inside the bubble chamber and the all particles were followed through the bubble chamber and the ISPF. The appropriate bubble chamber measured errors for tracks were assigned.

It was assumed that the ISPF covers 2π radians in the azimuth and $\pm 45^\circ$ in the vertical plane as it is shown in Fig. 1. We also assumed that the ISPF detects only γ 's with the energy greater than 500 MeV and its detection efficiency equals 99%. The ISPF energy resolution for a single was taken in the form

$$\frac{d(E_\gamma)}{E_\gamma} = \frac{0.33}{\sqrt{E_\gamma}}$$

where E_γ - energy of γ in GeV.

We have investigated the characteristics of the measured hadronic energy flow for the bubble chamber with and without ISPF. Figure 11 shows normalized distributions of the measured fraction of total hadronic energy

$$r = \frac{E'_h - E_h}{E_h}$$

for the bare bubble chamber and for the BC+ISPF hybrid system integrated over the hadronic energy range of (1-600) GeV. Figure 12 shows the average value and the resolution of r for the bare bubble chamber and for the BC+ISPF as a function of the total hadronic energy.

The use of the bubble chamber together with the ISPF essentially improve the accuracy of total hadronic energy determination. At $E_h \sim 100$ GeV the hybrid system detects 95% of the total hadronic energy with an accuracy $\sim 10\%$, while the bare bubble chamber detects only 70% of the hadronic energy with $\sim 23\%$ accuracy.

Since the ISPF records only two coordinates of photon showers in the azimuthal plane it is impossible to determine the dip angle of the γ -quantum. The unknown angle is obtained using the minimization of the following square form:

$$S = \frac{(P_z^{vis} + \Sigma P_z^\gamma)^2}{\sigma_z^2} + \frac{(P_y^{vis} + \Sigma P_y^\gamma)^2}{\sigma_y^2}$$

where p_z^{vis} and p_y^{vis} are the z and y components of the total momentum of a neutrino event measured in the bubble chamber; σ_z and σ_y are the errors of the p_z^{vis} and p_y^{vis} , respectively; p_z^γ and p_y^γ are the correspondent components fo the γ momentum.

The distributions of the angle δ between the true and the measured directions of the hadronic system for the bare bubble chamber and the BC+ISPF system are shown in Fig. 13. The energy dependences of the resolution for the direction of hadronic shower in both cases are shown in Fig. 14. At the $E_h \sim 100$ GeV the angle resolution is ~ 5 mrad for the BC+ISPF system and ~ 15 mrad for the bare bubble chamber.

REFERENCES

- ¹ Fermilab experiments E-45, E-28, E-172, E-380, E-338, E-546, E-545, E-1A, E-482. CERN experiments WA14, WA16, WA24, WA52, WA54.
- ² Fermilab experiments E-53A, E-180, E-542, E-310, E-616. CERN experiments WA1, WA18, WA21, WA25, WA47, WA59.
- ³ Ju. M. Antipov and S. P. Denisov, "A New Internal Picket Fence and Electromagnetic Energy Measurements in the 15-ft Bubble Chamber," Note presented at the workshop on Tevatron Neutrino and Muon Facilities, held at Fermilab 9-12, January 1980.
- ⁴ F. Harris, V. Z. Peterson, and M. Atac, U. H. Internal Report 26-76, 1976.
- ⁵ M. L. Stevenson, Paper Submitted to the Topical Conference on Neutrino Physics at Accelerators, Oxford, July 1978.
- ⁶ R. J. Cence et al., Nuclear Instr. Methods 138, 245 (1976).
- ⁷ J. Wolfson, Talk given on Neutrino Bubble Chamber Physics Workshop at Tevatron Energies, ANL, October 1979.
- ⁸ C. G. Callan and D. J. Crocc, Phys. Lett. 22, 156 (1979).
- ⁹ R. P. Feynman, Photon-Hadron Interactions (W. A. Benjamin, Readings, Massachusetts, 1972).
- ¹⁰ G. R. Farrar, D. R. Jackson, Phys. Rev. Lett. 35, 1416 (1975).
- ¹¹ A. Bodek et al., Preprint SLAC-Pub-2248, 1979.
- ¹² L. Anderson et al., Preprint FERMILAB-Pub-79/3-EXP, 1979.
- ¹³ P. C. Bosetti et al., Nucl. Phys. B142, 1 (1978).
- ¹⁴ W. A. Bardeen et al., Phys. Rev. D18, 3398 (1978).

- ¹⁵ A. DeRujula, J. Ellis, E. G. Floratos, and M. K. Gaillard, Nucl. Phys. B138, 387 (1978).
- ¹⁶ P. Binetruy, G. Girardi, Nucl. Phys. B155, 150 (1979).
- ¹⁷ R. D. Peccei, R. Ruckl, Phys. Lett. 84B, 35 (1979).
- ¹⁸ I. I. V. Bigi, Phys. Lett. 86B, 57 (1976).
- ¹⁹ P. Mazzanti et al., Phys. Lett. 81B, 219 (1979).
A. Mendez, Nucl. Phys. B145, 199 (1978)
- ²⁰ N. Schmitz, Rapporteurs talk at the Lepton Photon Conference, Fermilab, 1979.
- ²¹ D. H. Perkins, Oxford preprint 2-79 (1979).
- ²² W. G. Scott, paper presented at 7th Intern. Winter Meeting on Fundamental Physics, Segovia, Spain (1979).
- ²³ J. F. Owens, Phys. Lett. 76B, 85 (1978). T. Uematsu, Phys Lett. 79B, 97 (1978).
- ²⁴ N. Sakai, Phys. Lett. 85B, 67 (1979).
- ²⁵ M. J. Murtagh, Rapporteurs talk at the Lepton Photon Conference, Fermilab, 1979.
- ²⁶ R. J. N. Phillips, Nucl. Phys. B153, 475 (1979).
- ²⁷ J. Ellis et al., Nucl. Phys. B131, 285 (1977). C. H. Albright et al., Phys. Rev. D17, 2383 (1978). M. Kobayashi, T. Maskawa, Prog. Pheor. Phys., 49, 652 (1973).
- ²⁸ T. Hansl et al., Nucl. Phys. B142, 381 (1978). A. Benvenuti et al., Phys. Rev. Lett. 42, 1024 (1979)
- ²⁹ J. G. H. deGroot et al., Preprint Saclay DPhPE79-06 (1979).
- ³⁰ S. L. Glashow, J. Illiopoulos, and L. Maiani, Phys. Rev. D2, 1285 (1970).

- ³¹ L. M. Sehgal, Summary talk given at SPSC Workshop on Neutrino Physics, CERN, November, 1978.
- ³² W. A. Venus, H. W. Wachsumth. TL-L/Int., 73-2; RL-73-137 (1973). N. A. Nezhick, Nuclear Science, NS-22, N3, 1479 (1975).
- ³³ V. I. Voronov et al., Nucl. Instrum. Meth. 105, 147 (1972).
- ³⁴ J. Grimson, S. Mori, TM-824, Fermilab (1978).
- ³⁵ S. Mori, TM-720, Fermilab (1977).
- ³⁶ S. Van der Meer, CERN 62-16, (1962).
- ³⁷ E. Regenstreif, CERN 64-41 (1964).
- ³⁸ D. S. Baranov and V. L. Rykov, Preprint IHEP 79-170, Serpukhov, 1979.
- ³⁹ D. C. Carey, and V. A. White, Fermilab Internal Report, NUADA (1975).
- ⁴⁰ The Proceedings of the October 1978 E-180 Collaboration Meeting FIIM group.
- ⁴¹ K. A. Akerloff et al., Preprint IHEP 77-86, Serpukhov, 1977.
- ⁴² R. J. Stefanski, and H. B. White, FN -292, 1060.0 (1979).
- ⁴³ B. Aubert et al., Prepr. Fermilab-Conf-75/31.
- ⁴⁴ T. B. Kirk, Neutrino-Muon Workshop, Fermilab, January 1980.
- ⁴⁵ R. D. Field, and R. P. Feynman, Phys. Rev. D15, 2590 (1977).
- ⁴⁶ J. Bell et al., Phys. Rev. D19, (1979).
- ⁴⁷ E. L. Woods, Fermilab TM-573, 1975.

TABLE I

Expected charged-current event yields in the 17m^3 fiducial volume for 1 TeV protons. (10^{13} proton on target, deuterium filling.)

E (GeV)	Neutrino Exposures	Antineutrino Exposures
10-50	0.208	0.0525
50-100	0.203	0.0371
100-150	0.055	0.0091
150-200	0.035	0.0045
200-250	0.025	0.0027
250-300	0.016	0.0014
300-350	0.010	0.0007
350-400	0.006	-
400-450	0.004	-
450-550	0.002	-
Total	0.562	0.108

TABLE IIa.

Relative contribution of background antineutrino flux as a function of the FW current, proton beam radius $\sigma_p = 1$ cm.

I_w (KA)	0.5	1.0	1.5	2.0	3.0
$\frac{\int \frac{dN_{\bar{\nu}}}{dE_{\bar{\nu}}} dE_{\bar{\nu}}}{\int \frac{dN_{\nu}}{dE_{\nu}} dE_{\nu}}$	0.170	0.085	0.050	0.030	0.018
$\frac{dN_{\bar{\nu}}/dE_{\bar{\nu}}}{dN_{\nu}/dE_{\nu}} (E_{\nu} = 10)$	0.245	0.130	0.070	0.050	0.026
$\frac{dN_{\bar{\nu}}/dE_{\bar{\nu}}}{dN_{\nu}/dE_{\nu}} (E_{\nu} = 100)$	0.260	0.130	0.080	0.060	0.037
$\frac{dN_{\bar{\nu}}/dE_{\bar{\nu}}}{dN_{\nu}/dE_{\nu}} (E_{\nu} = 200)$	0.130	0.090	0.055	0.035	0.018
$\frac{dN_{\bar{\nu}}/dE_{\bar{\nu}}}{dN_{\nu}/dE_{\nu}} (E_{\nu} = 300)$	0.090	0.050	0.030	0.023	0.010

TABLE IIb.

Relative contribution of background antineutrino flux as a function of the proton beam radius: $\sigma_p, I_w = 2 \text{ KA}$.

σ_p (cm)	0.1	0.25	0.5	1.0	2.0	3.0
$\int \frac{dN_{\bar{\nu}}}{dE_{\bar{\nu}}} dE_{\bar{\nu}}$	0.018	0.016	0.020	0.030	0.060	0.085
$\int \frac{dN_{\nu}}{dE_{\nu}} dE_{\nu}$						
$\frac{dN_{\bar{\nu}}/dE_{\bar{\nu}}}{dN_{\nu}/dE_{\nu}} (E_{\nu}=10)$	0.035	0.025	0.035	0.050	0.088	0.011
$\frac{dN_{\bar{\nu}}/dE_{\bar{\nu}}}{dN_{\nu}/dE_{\nu}} (E_{\nu}=100)$	0.035	0.029	0.035	0.060	0.110	0.180
$\frac{dN_{\bar{\nu}}/dE_{\bar{\nu}}}{dN_{\nu}/dE_{\nu}} (E_{\nu} = 200)$	0.015	0.013	0.019	0.040	0.067	0.085
$\frac{dN_{\bar{\nu}}/dE_{\bar{\nu}}}{dN_{\nu}/dE_{\nu}} (E_{\nu} = 300)$	0.005	0.007	0.010	0.023	0.040	0.057

TABLE III

Parametrization for the Al target with $l = 0.6$ m, $r = 0.03$ m.

	a_1	a_2	a_3	a_4	a_5	a_6	a_7
π^+	4.51	4.41	7.37	7.88	0.495	13.2	2.96
π^-	3.66	4.08	4.0	7.07	0.608	14.0	3.38
K^+	0.256	3.41	5.25	6.25	0.975	11.0	2.97
K^-	0.288	8.69	11.2	8.65	0.810	14.4	3.97

TABLE IVa

Relative fluxes for neutrino beam at the 15-ft bubble chamber normalized to neutrino flux with the horn (%)

E_{ν} (GeV)	ν_{μ} focusing			$\bar{\nu}_{\mu}$ defocusing		
	horn	horn + plug	FW	horn	horn + plug	FW
10-400	100	73	91	15	1.7	2.5
10-50	73	56	66	9.8	1.35	1.6
50-100	17.5	11.5	16	3.7	0.25	0.6
100-200	7	4.3	7	1.3	0.085	0.25
200-300	2	1.0	1.5	0.2	0.015	0.04
300-400	0.5	0.2	0.5	0.06	0.0025	0.01

TABLE IVb

Relative event rates for neutrino beam at the 15-ft bubble chamber, normalized to neutrino event yield with the horn (%)

E_{ν} (GeV)	ν_{μ} focusing			$\bar{\nu}_{\mu}$ defocusing		
	horn	horn + plug	FW	horn	horn + plug	FW
10-400	100	68	93	17	1.5	2.7
10-50	40.5	32.7	37	6	0.75	0.82
50-100	25.5	16.7	23.5	5.5	0.40	0.82
100-200	21.5	12.5	19.5	4	0.25	0.77
200-300	8.5	4.5	8.5	1.	0.08	0.23
300-400	4.0	1.6	4.5	0.5	0.02	0.06

TABLE Va

Relative fluxes for the antineutrino beam at the 15-ft bubble chamber normalized to antineutrino flux with the horn (%)

$E_{\bar{\nu}}$ (GeV)	$\bar{\nu}_{\mu}$ focusing			ν_{μ} defocusing		
	horn	horn + plug	FW	horn	horn + plug	FW
10-400	100	78	112	41	5	8.3
10-50	78.5	65	90	21.7	3.4	4.3
50-100	16.5	11	17	11.2	0.9	2.1
100-200	4.3	2	4.4	5.8	0.5	1.4
200-300	0.6	0.8	0.5	1.6	0.16	0.37
300-400	0.1	0.04	0.1	0.7	0.04	0.13

TABLE Vb

Relative event rates for antineutrino beam at the 15-ft bubble chamber, normalized to antineutrino event yield with the horn (%)

$E_{\bar{\nu}}$ (GeV)	$\bar{\nu}_{\mu}$ focusing			ν_{μ} defocusing		
	horn	horn + plug	FW	horn	horn + plug	FW
10-400	100	70	107	71	6.5	14.5
10-50	54	43	58.5	15.7	2.3	2.7
50-100	28	17.5	28.5	19.5	1.5	3.6
100-200	14	7.7	15	19.5	1.55	4.9
200-300	3	1.5	4	10.	0.85	2.3
300-400	1.	0.3	1.	6.3	0.30	1.0

TABLE VI

Wire length (m)	400
Wire radius (mm)	1
Decay pipe radius (cm)	45.7
Distance between wire suspensions (m)	~5-8
Wire draw strength (kG)	~100
Wire sagitta between suspensions (mm)	1-2
Inductance (H)	$\sim 0.5 \times 10^{-3}$
Resistance (Ω)	~3

TABLE VII

Cycle time (sec)	60
Number of fast spill pulses	1
Wire current length (msec)	2
Peak current (kA)	2
Voltage (kV)	6
Magnetic field storage energy $LI^2/2$ (kJ)	1
Dissipation energy I^2R per pulse (kJ)	24
Wire heating per pulse ($^{\circ}C$)	6
Average heating power (wt/m)	4
Wire average temperature ($^{\circ}C$)	50
Average consumed power (wt)	1600

FIGURE CAPTIONS

Fig. 1. General layout of the Fermilab 15-ft bubble chamber with the external devices.

Fig. 2. Neutrino fluxes obtained using the horn system and the wire focusing system.

Fig. 3. Antineutrino fluxes obtained using the horn system and the wire focusing system.

Fig. 4. Q^2 and x regions covered by the proposed experiment.

Fig. 5. Integral neutrino flux (curve 1) and the flux densities (curves 2-8) for different E_ν energies (10, 50, 100, 110, 200, 250, 300 GeV) as a function of the FW current.

Fig. 6. Neutrino flux (curve 1) and the flux densities (curves 2-10) as functions of the proton beam size σ_p for different E_ν energies (10, 50, 100, 150, 200, 250, 300, 350, and 400 GeV).

Fig. 7. Background antineutrino flux and the flux densities as functions of the FW current (see Fig. 5).

Fig. 8. Background antineutrino flux and the flux densities as functions of the proton beam size (see Fig. 6).

Fig. 9. Momentum spectra of the secondary mesons at 1 TeV proton energy (Al target, $\theta_{\text{prod}} < 40$ mrad).

Fig. 10. Comparison of meson production at 300 GeV/c from the Al target with the IHEP parametrization and the Stefanski-White⁴² parametrization (see text).

Fig. 11. Normalized distributions of the measured fraction of the total hadronic energy $r = (E_{h'} - E_h)/E_h$ for the bare bubble chamber and for the BC+ISPF.

Fig. 12. Average value and resolution of $r = (E_{h'} - E_h)/E_h$ for the bare bubble chamber and for the BC+ISPF.

Fig. 13. Distributions of the angle δ between the true and measured hadronic jet direction for the bare bubble chamber and for the BC+ISPF.

Fig. 14. Energy dependences of resolution for the hadronic jet direction for the bare bubble chamber and for the BC+ISPF.

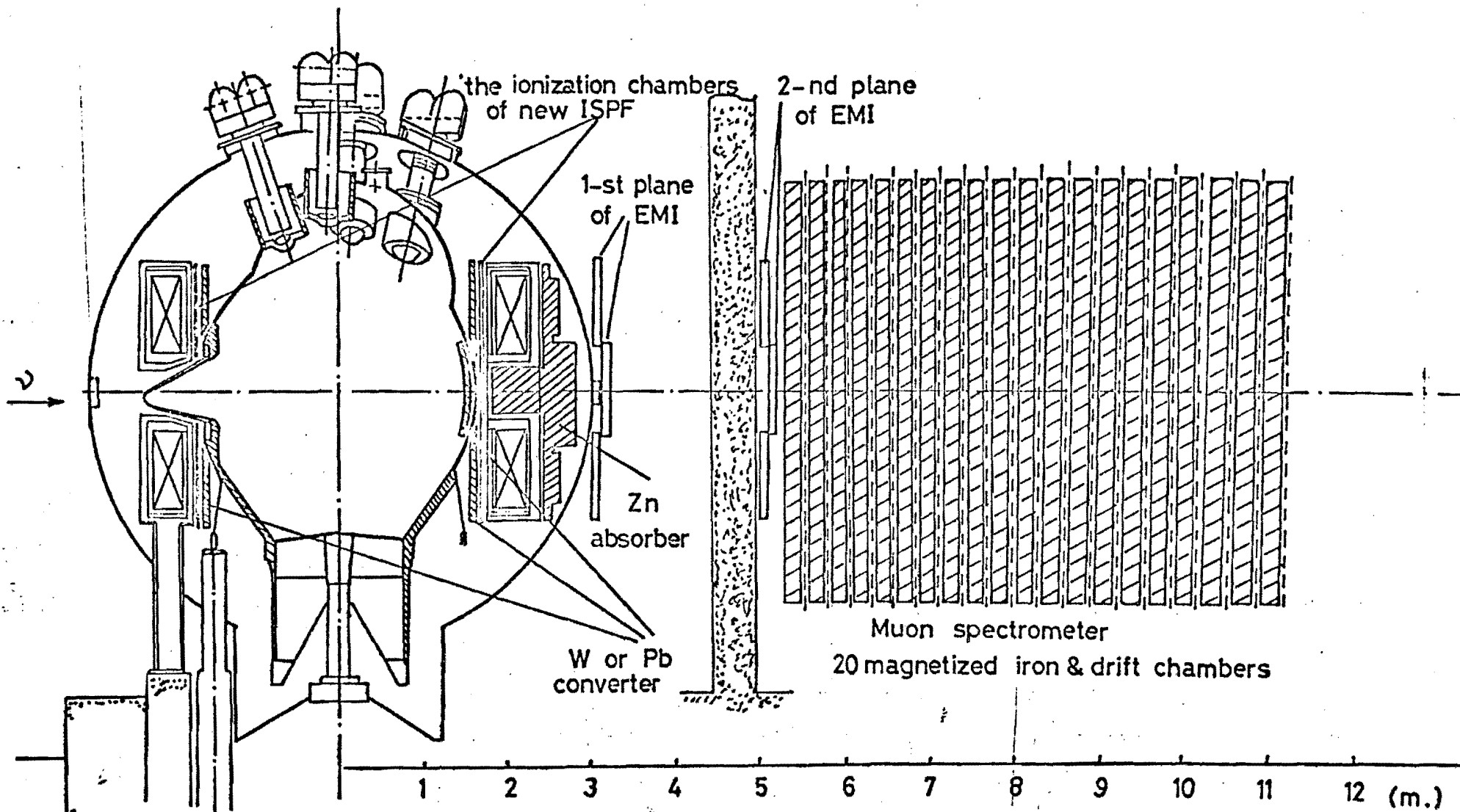


Fig. 1

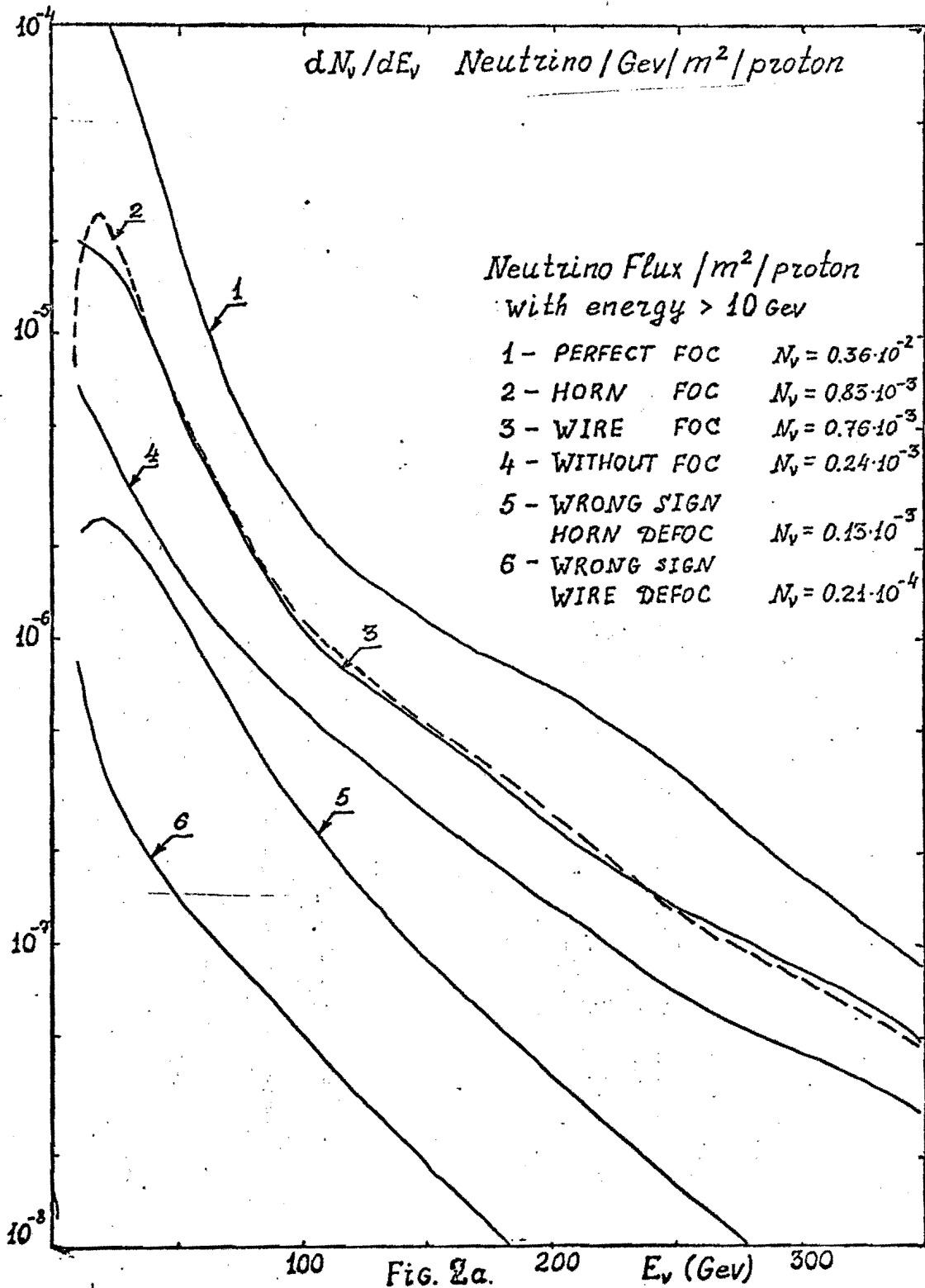
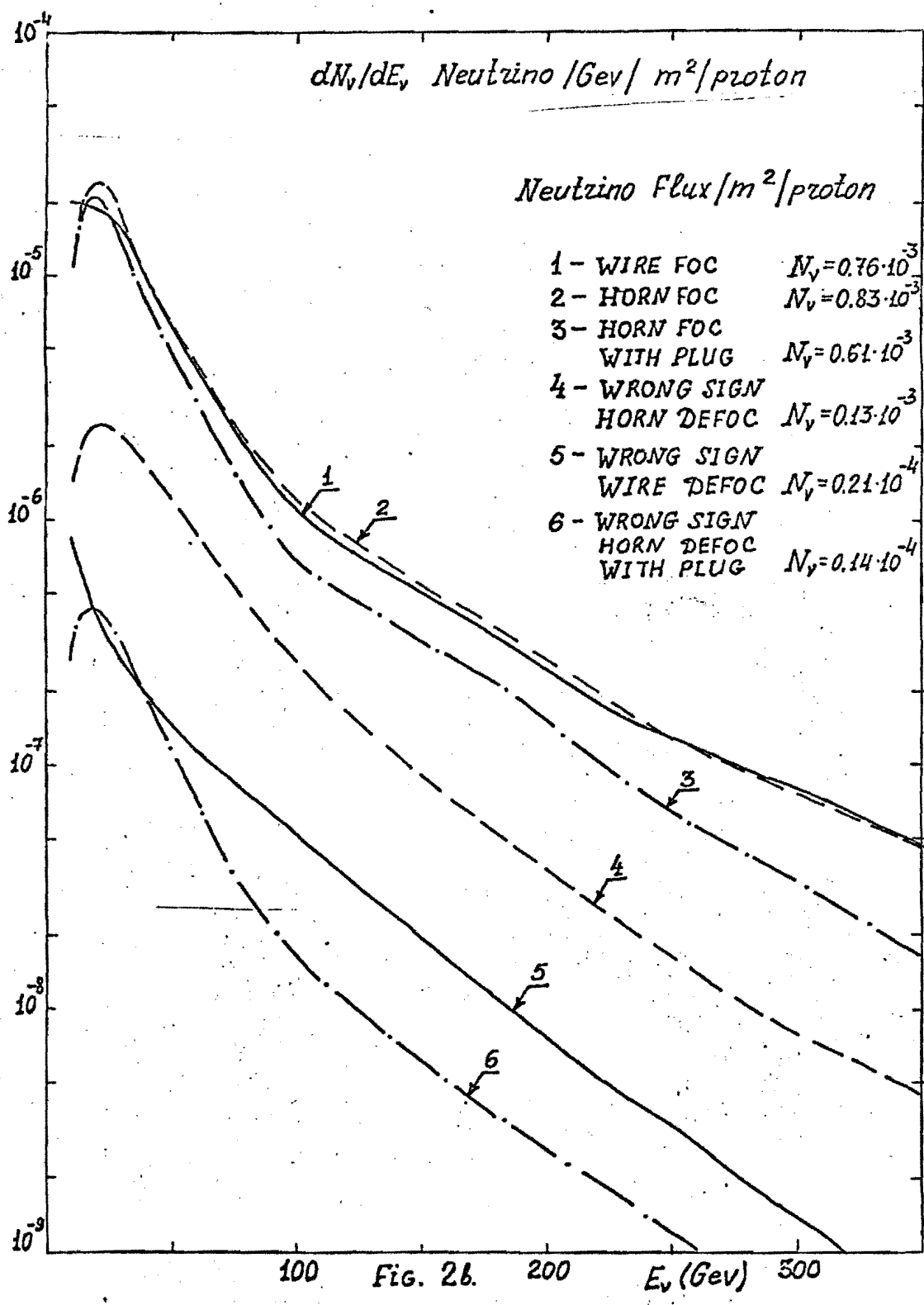
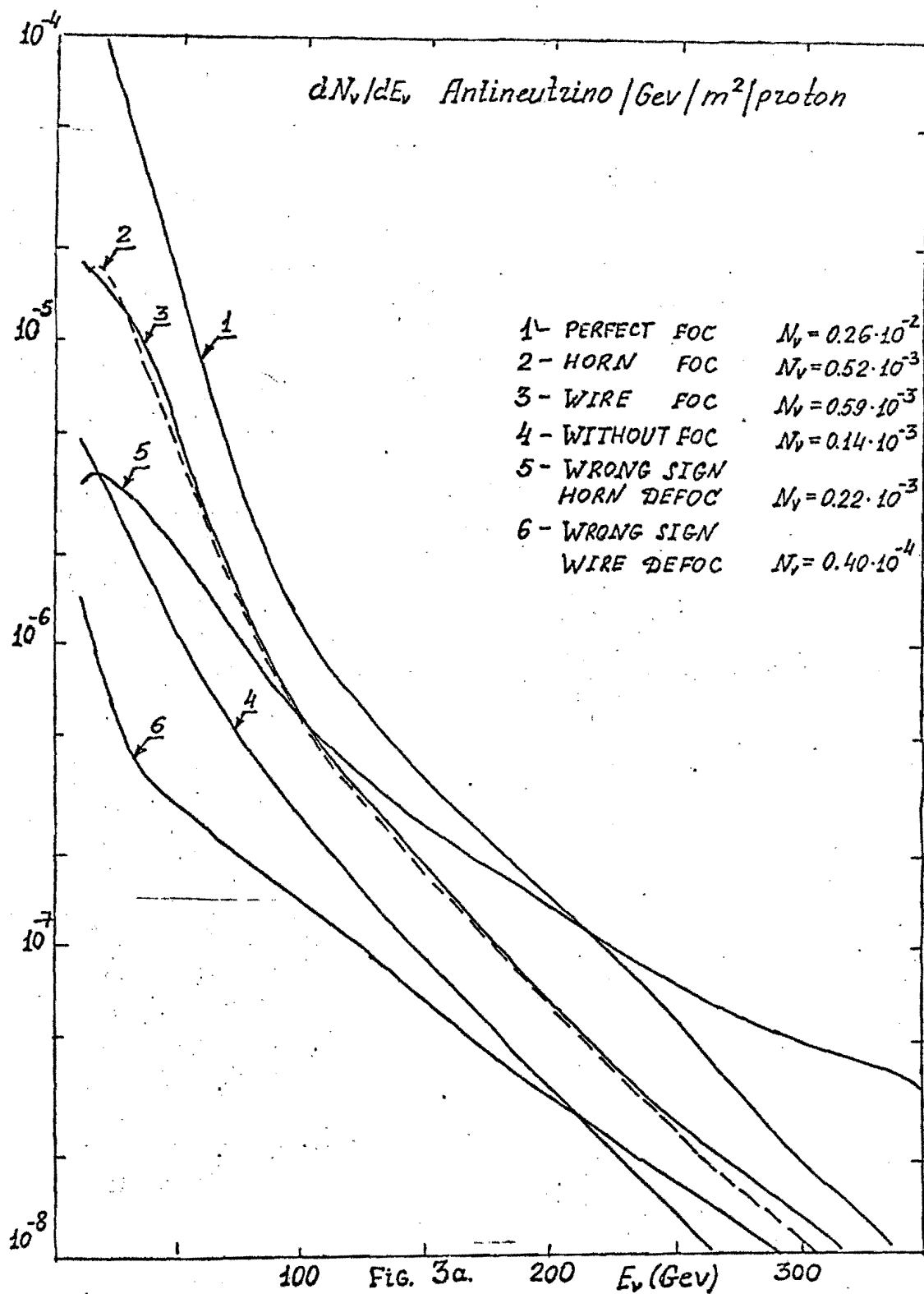
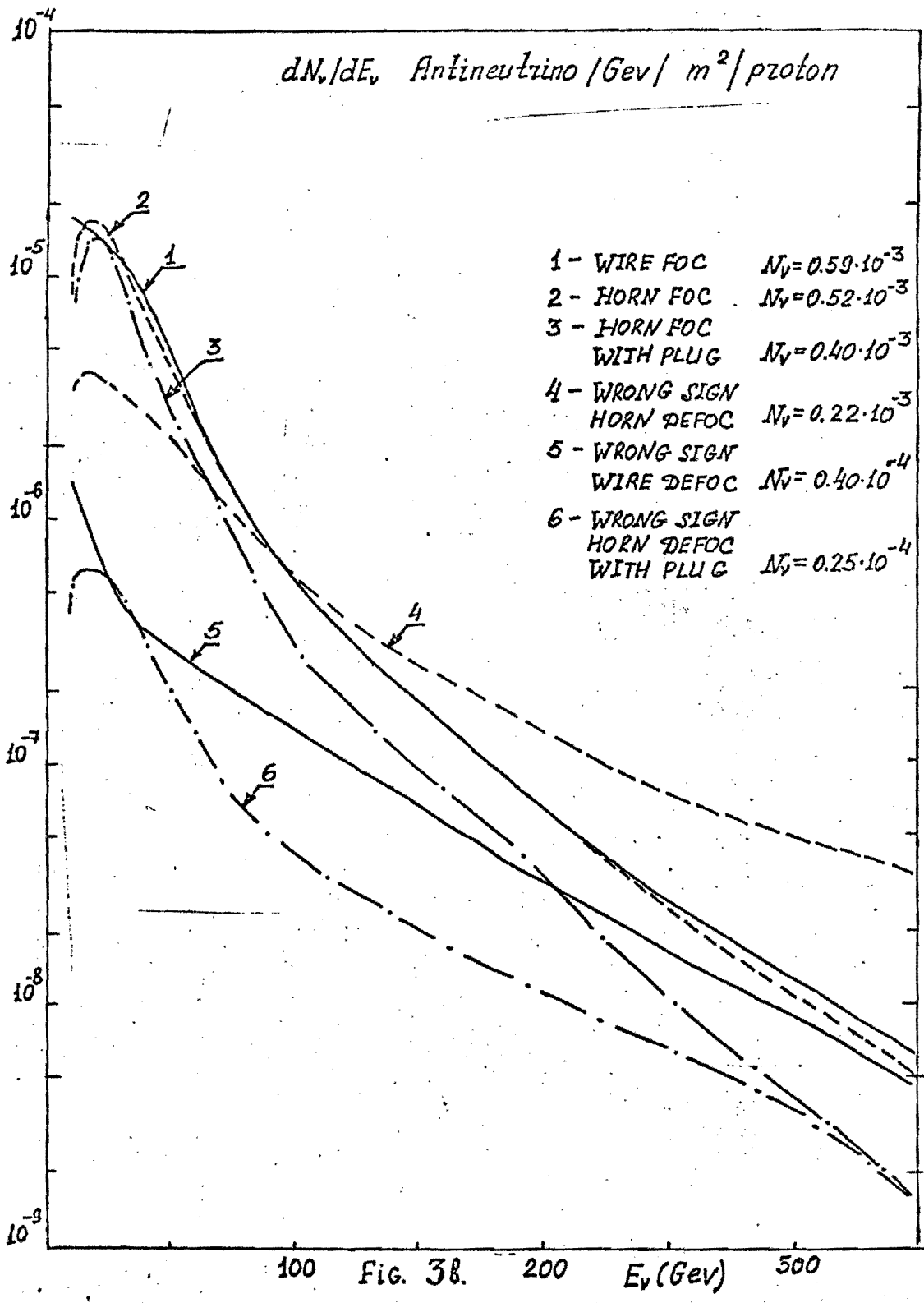


Fig. 2a.







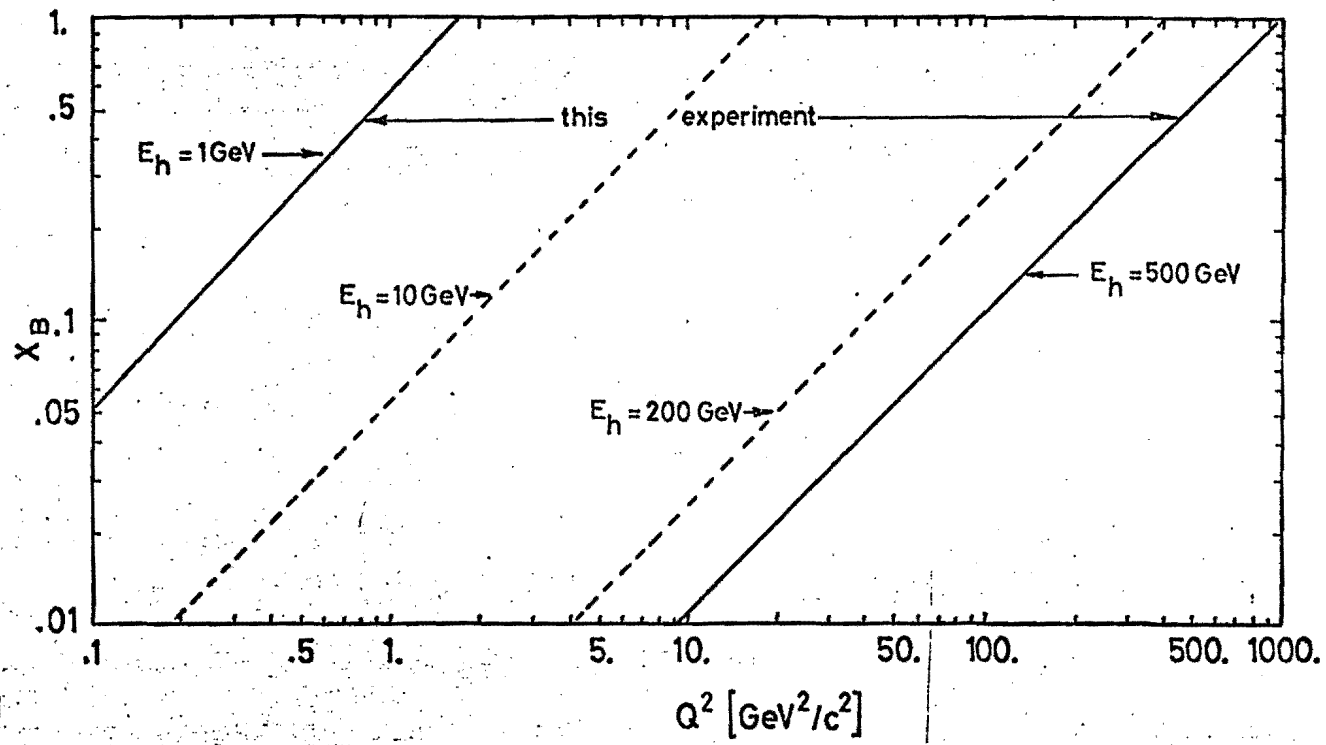


Fig. 4

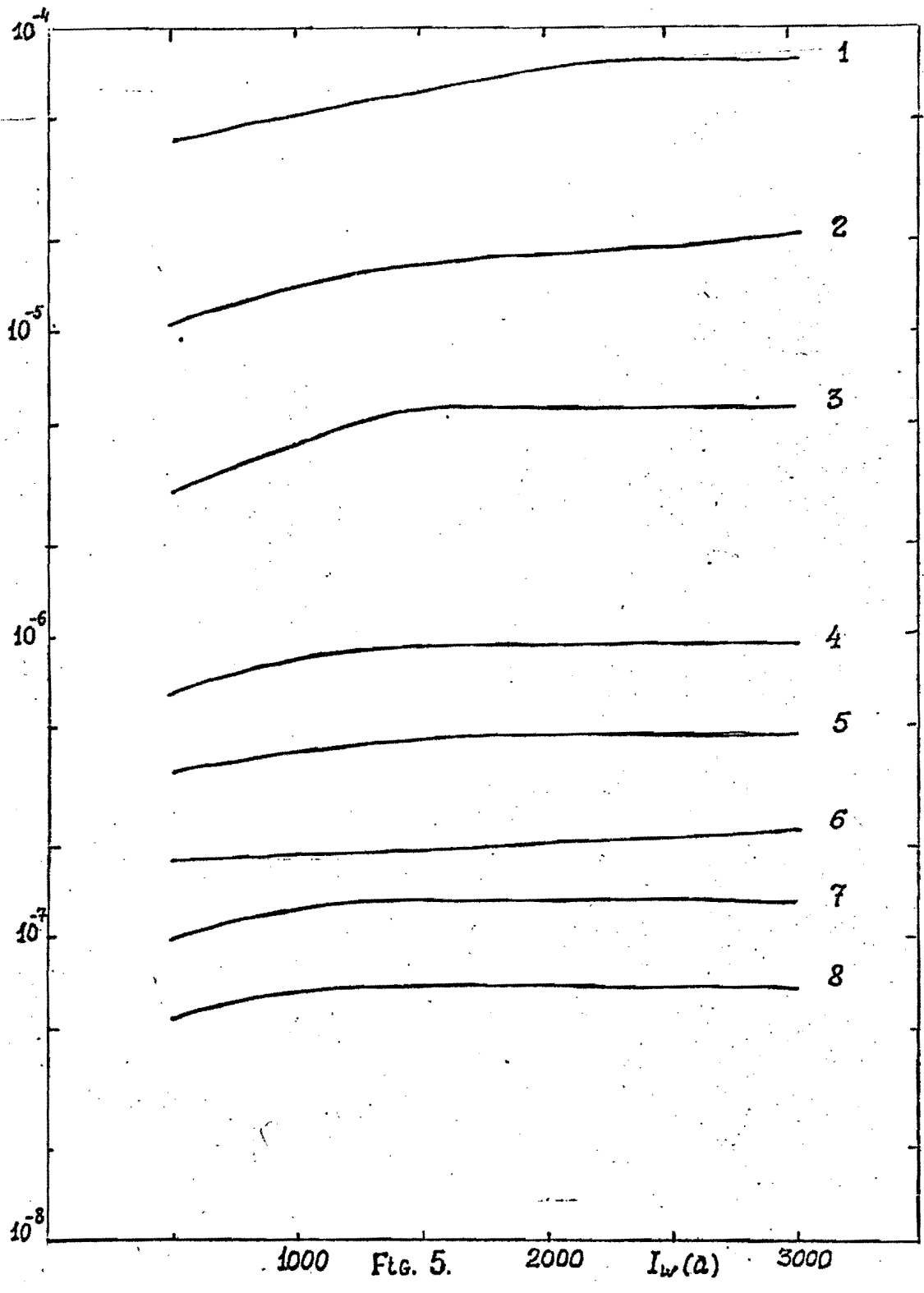
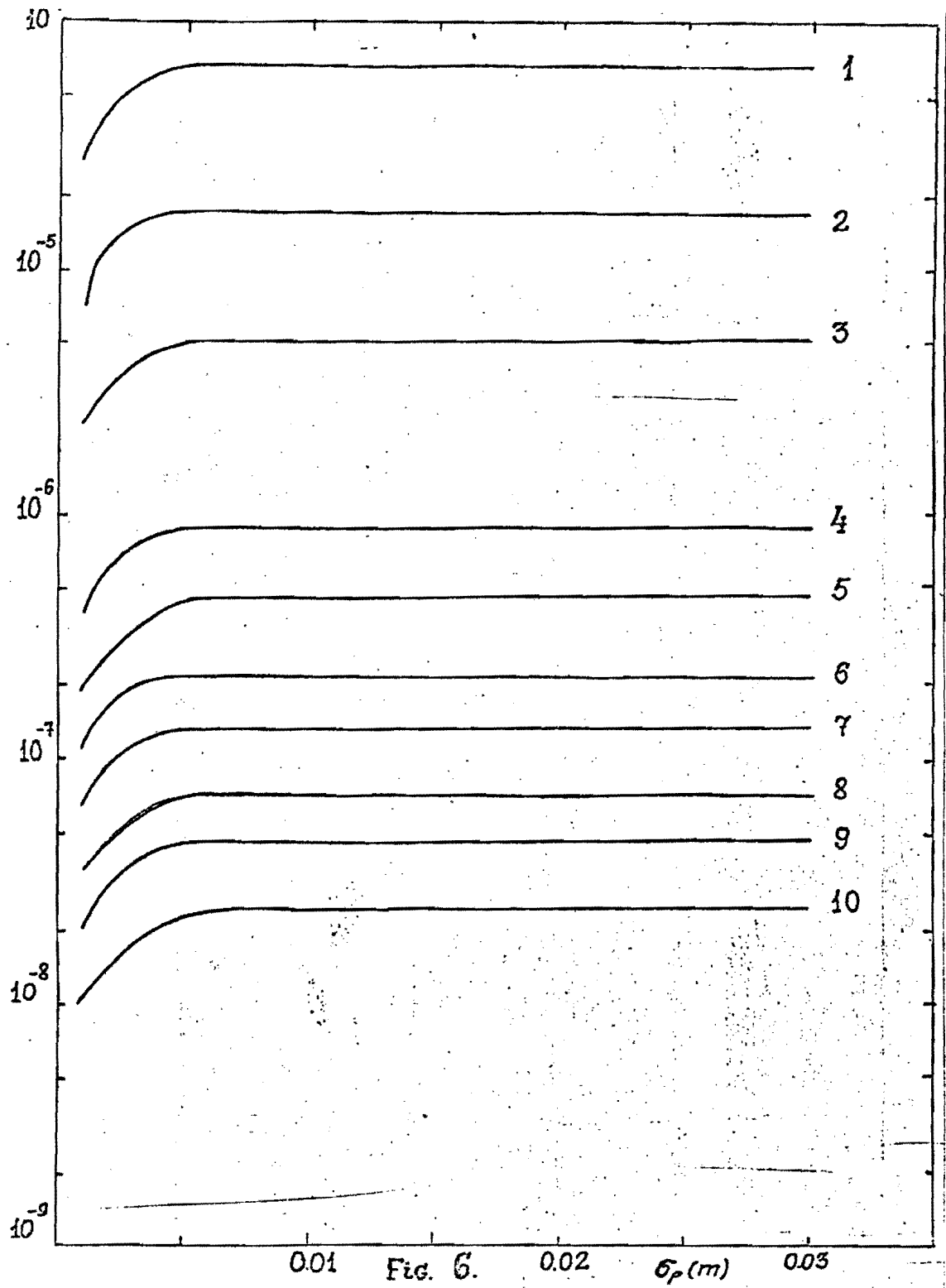
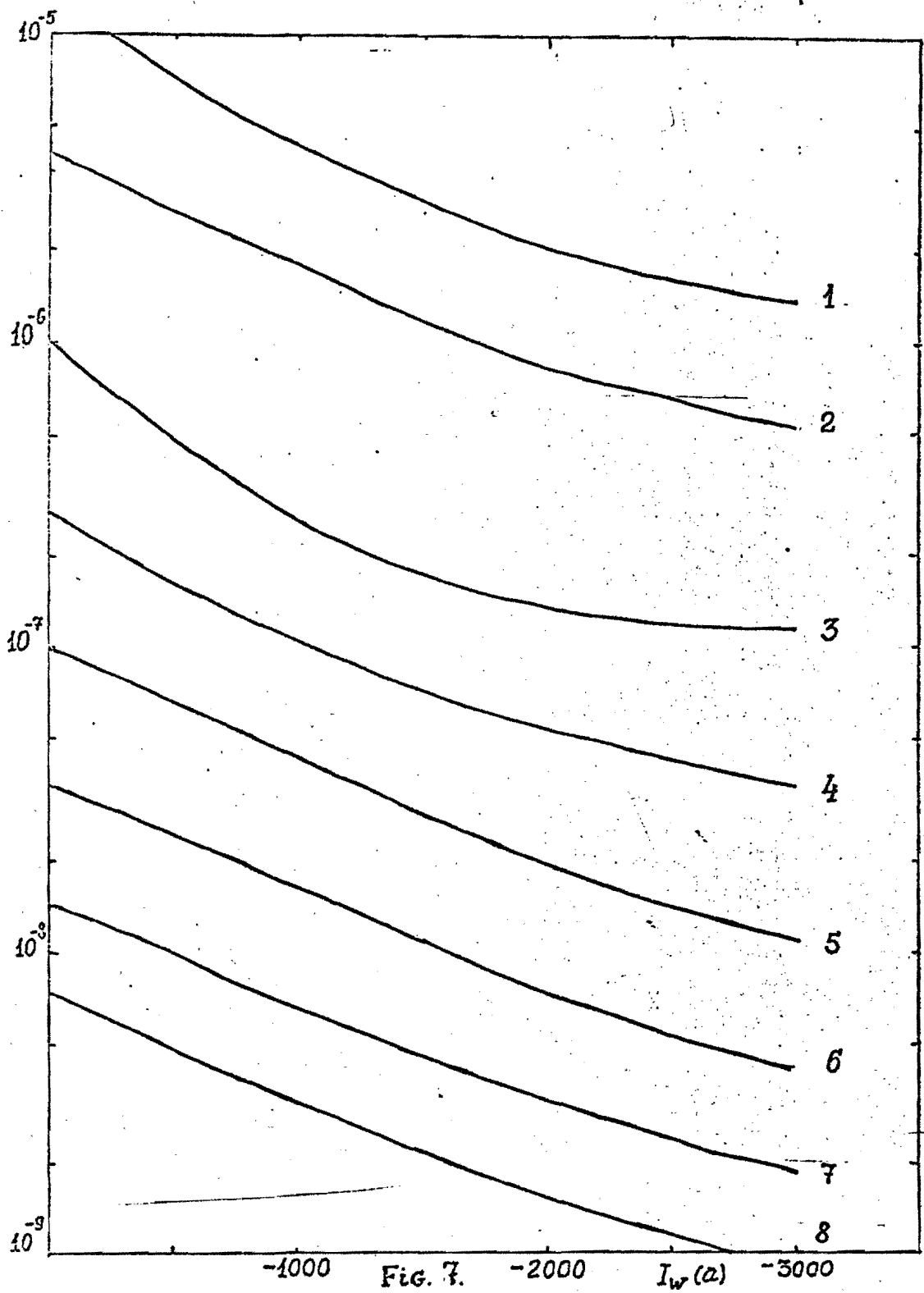
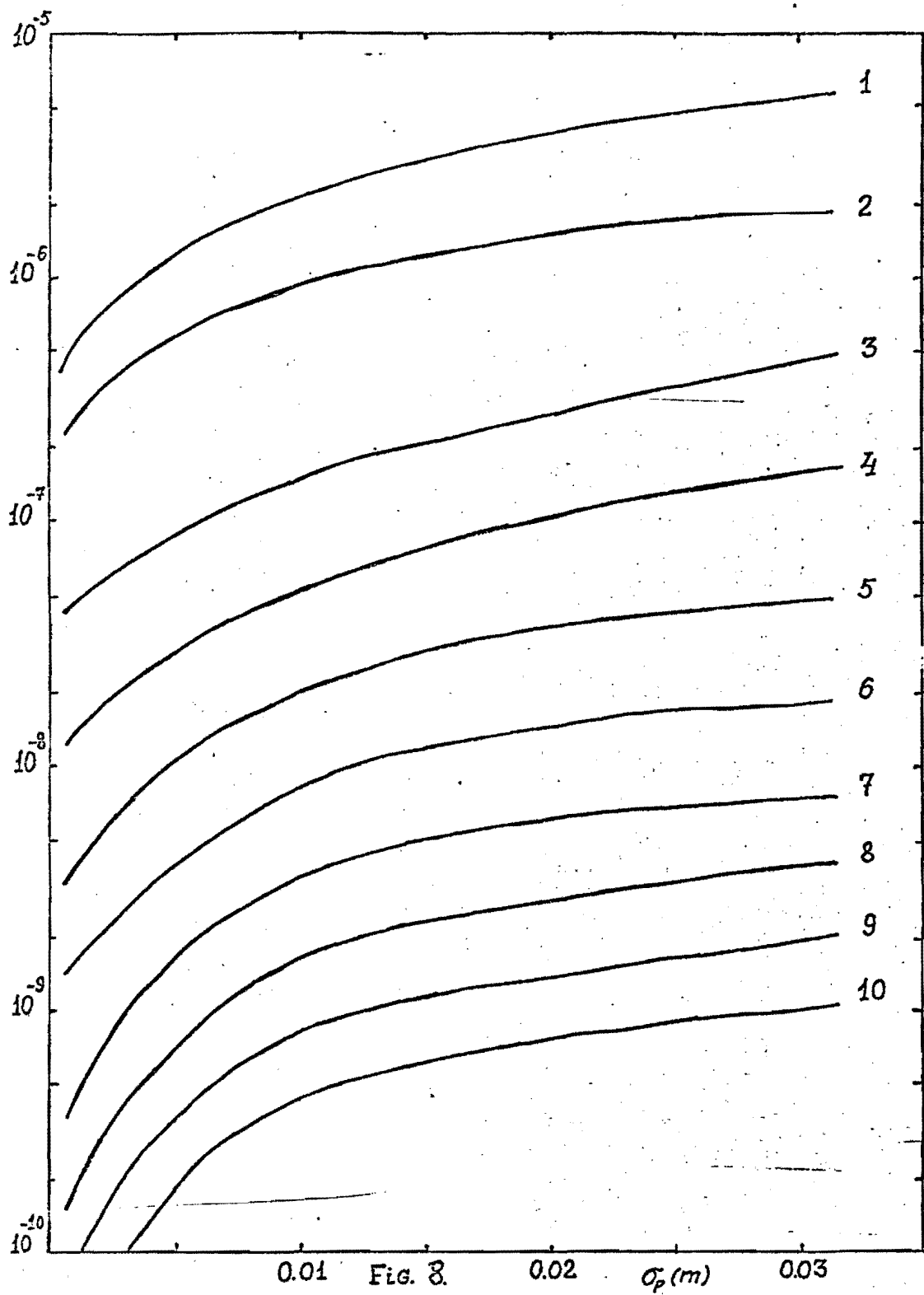


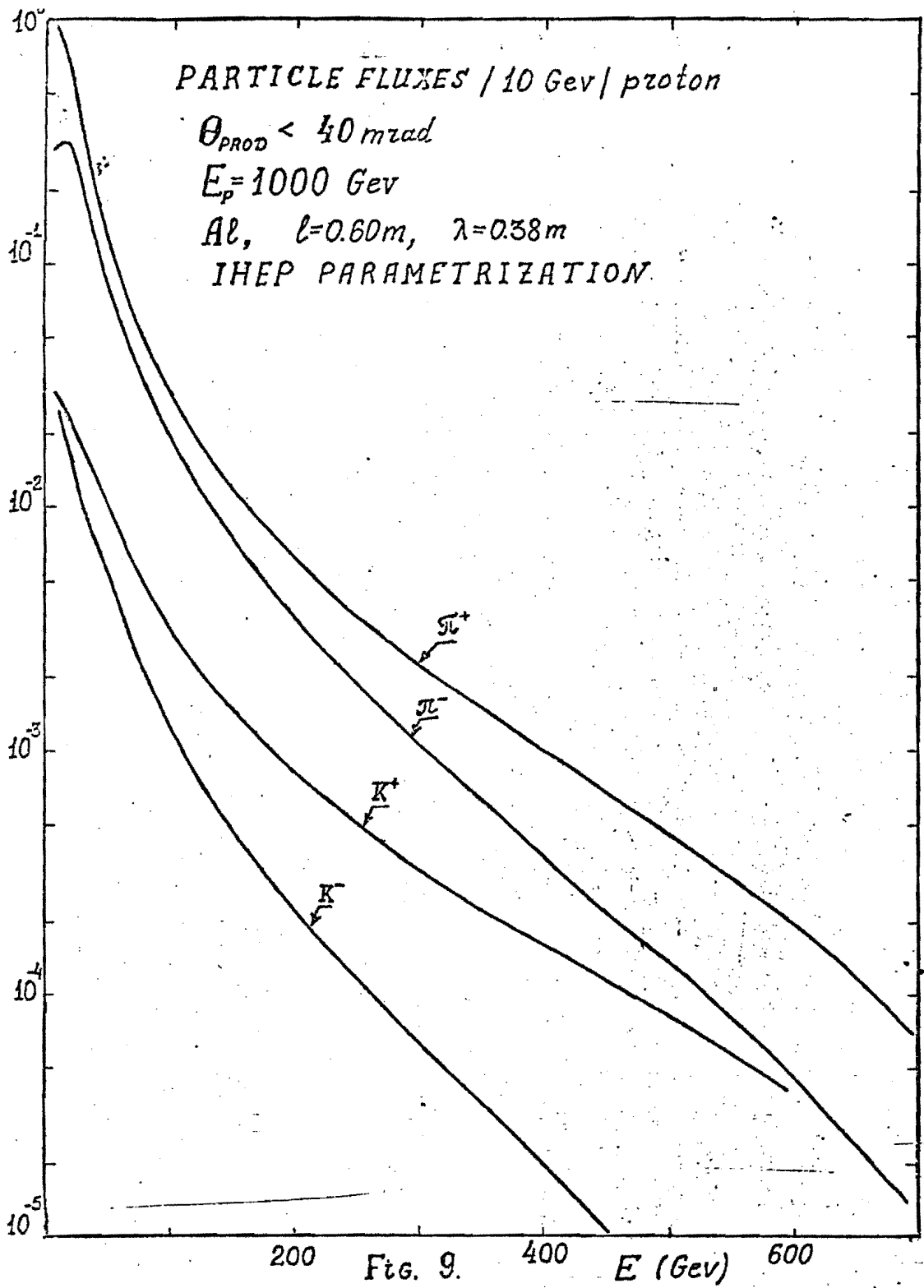
FIG. 5.

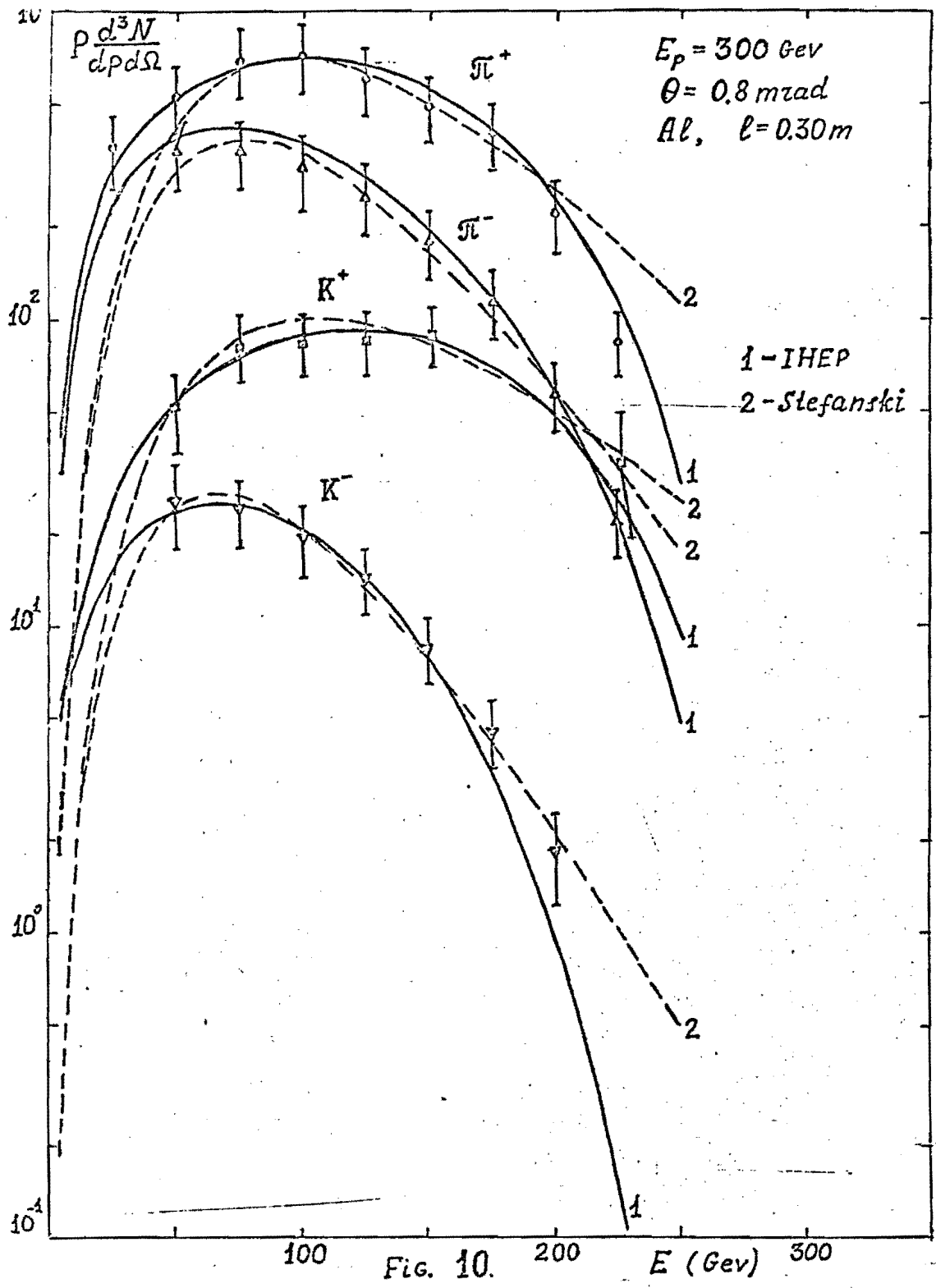
$I_w(a)$











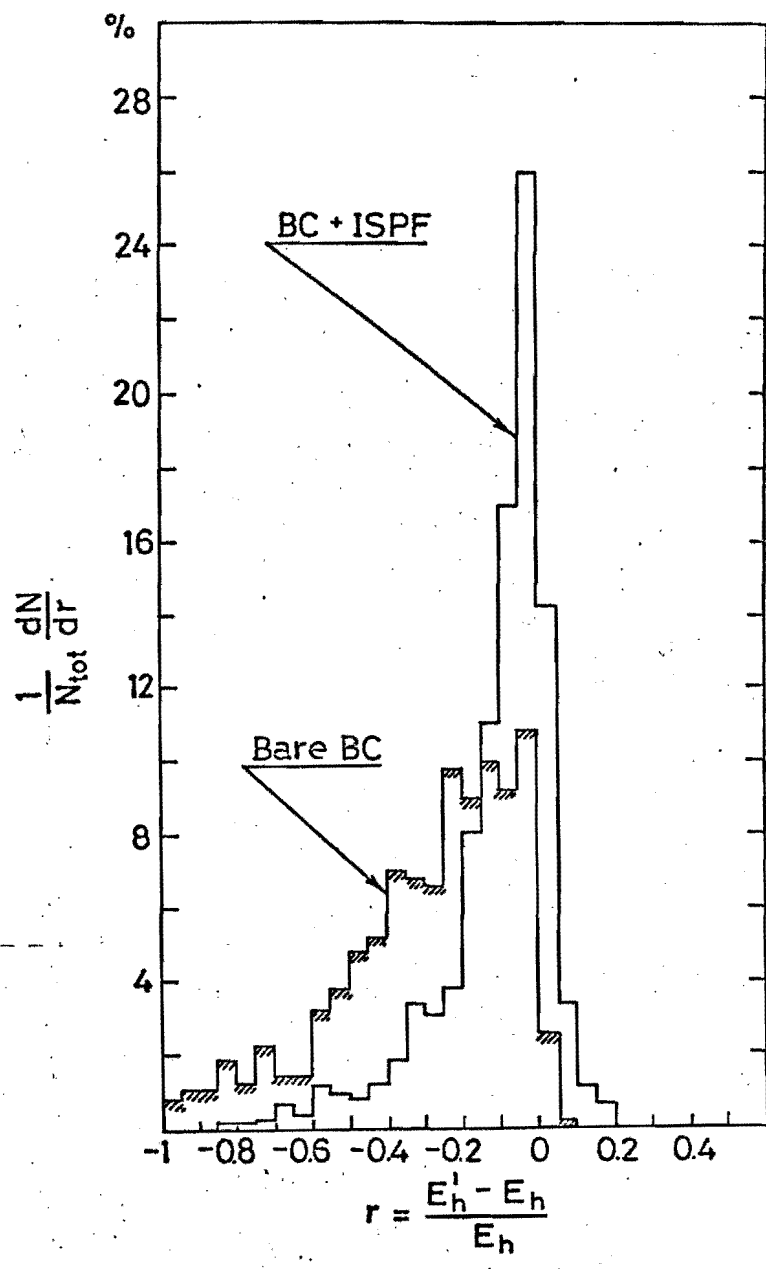


Fig. 11

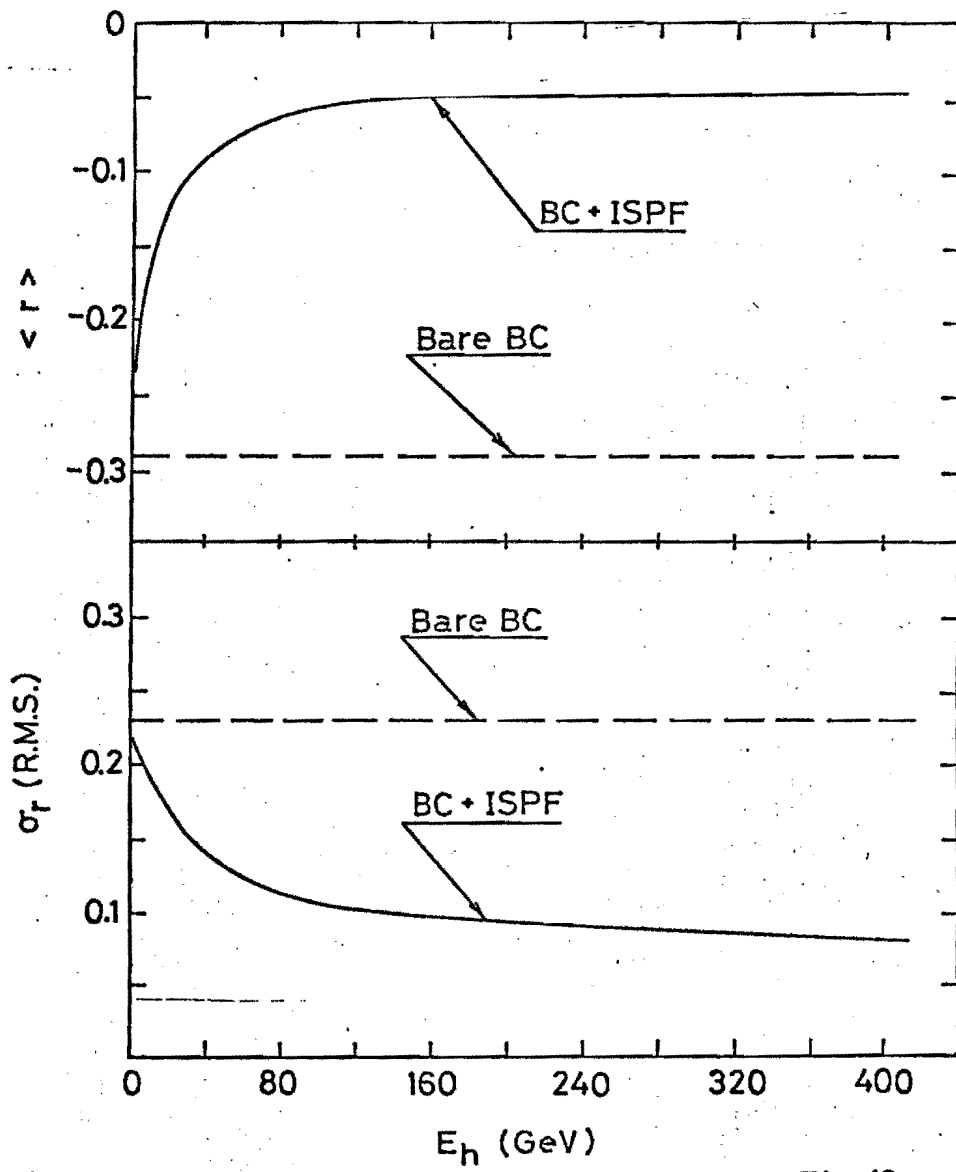


Fig. 12

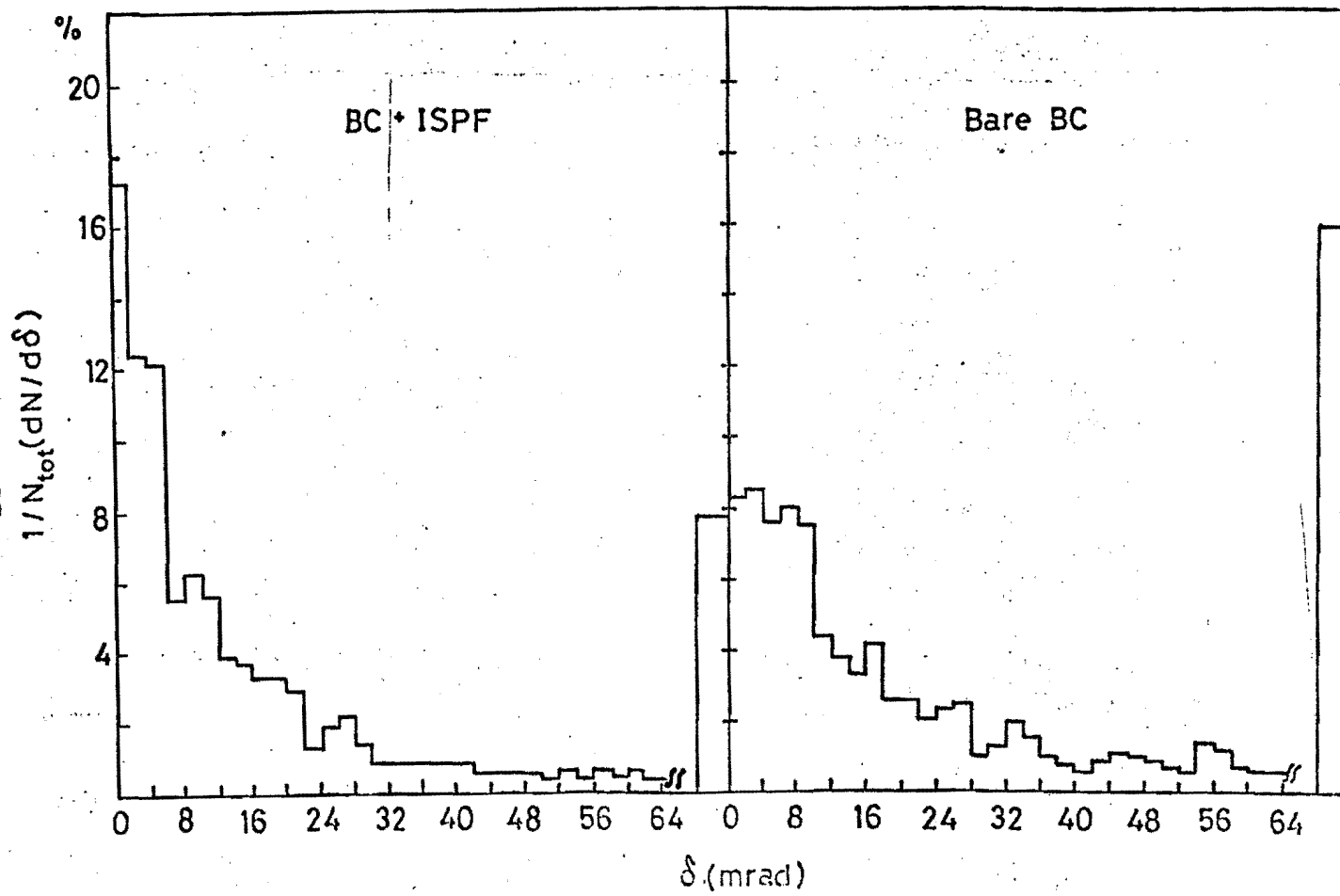


Fig. 13

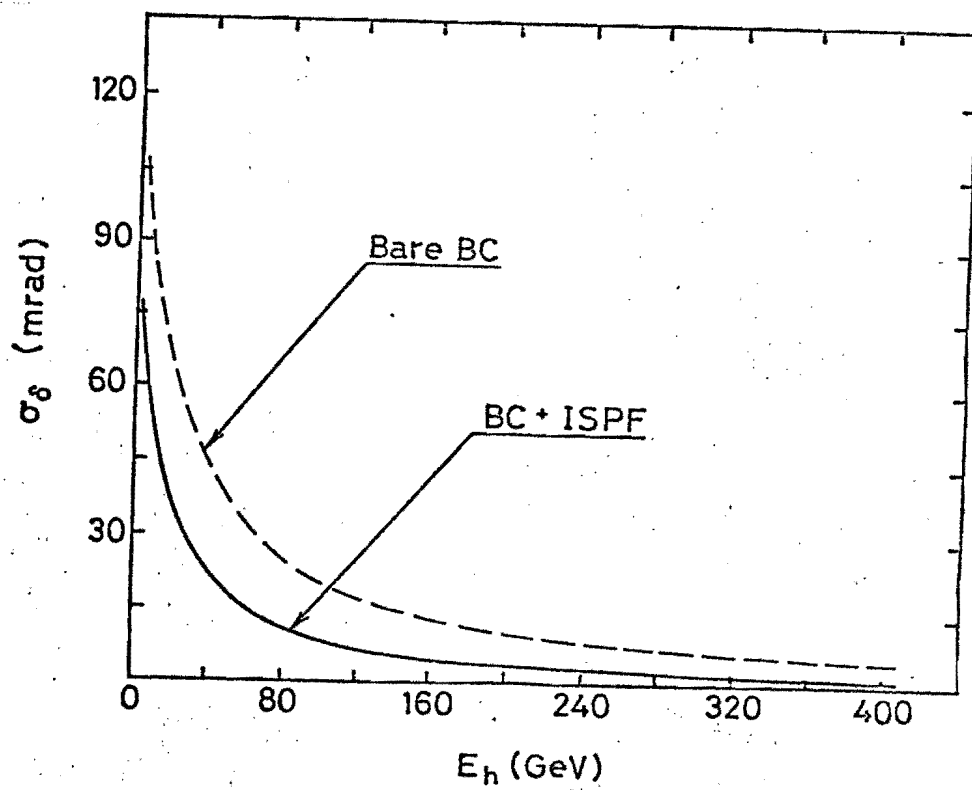


Fig. 14